

Here is a preprint (submitted manuscript) of the following paper:

Amicarelli A., S. Manenti, R. Albano, G. Agate, M. Paggi, L. Longoni, D. Mirauda, L. Ziane, G. Viccione, S. Todeschini, A. Sole, L.M. Baldini, D. Brambilla, M. Papini, M.C. Khellaf, B. Tagliaferro, L. Sarno, G. Pirovano; 2020; SPHERA v.9.0.0: a Computational Fluid Dynamics research code, based on the Smoothed Particle Hydrodynamics mesh-less method; Computer Physics Communications; DOI: 10.1016/j.cpc.2020.107157

Please refer to the published version of the manuscript:

<https://www.sciencedirect.com/science/article/pii/S0010465520300187?via%3Dihub>

SPHERA v.9.0.0: a Computational Fluid Dynamics research code, based on the Smoothed Particle Hydrodynamics mesh-less method

Andrea Amicarelli^{1,0}, Sauro Manenti², Raffaele Albano³, Giordano Agate¹, Marco Paggi⁴, Laura Longoni⁵, Domenica Mirauda³, Latifa Ziane⁶, Giacomo Viccione⁷, Sara Todeschini², Aurelia Sole³, Lara Martina Baldini^{5,1}, Davide Brambilla⁵, Monica Papini⁵, Mohamed Cherif Khellaf⁶, Bonaventura Tagliaferro⁷, Luca Sarno⁷, Guido Pirovano¹

¹Ricerca sul Sistema Energetico - RSE SpA, Department SFE, via Rubattino, 54, 20134, Milan, Italy

²Dipartimento di Ingegneria Civile e Architettura (DICAr), via Ferrata 3, 27100 Pavia, Italy

³School of Engineering, University of Basilicata, Potenza, Italy

⁴IMT School for Advanced Studies Lucca, Piazza San Francesco 19, 55100 Lucca, Italy

⁵Environmental and Civil Engineering Department, Politecnico di Milano, P.za Leonardo da Vinci 32, 20133 Milan, Italy

⁶LEGHYD laboratory, faculty of civil engineering, University of Sciences and Technology Houari Boumediene, Algiers, Algeria

⁷Department of Civil Engineering, University of Salerno, via Giovanni Paolo II, 132, 84084 Fisciano, Italy

⁰Corresponding author

andrea.amicarelli@rse-web.it sauro.manenti@unipv.it raffaele.albano@unibas.it giordano.agate@rse-web.it

marco.paggi@imtlucca.it laura.longoni@polimi.it domenica.mirauda@unibas.it latifa.ziane@hotmail.fr

gviccione@unisa.it sara.todeschini@unipv.it aurelia.sole@unibas.it lara_baldini@virgilio.it

davide.brambilla@polimi.it monica.papini@polimi.it mckhellaf@yahoo.fr btagliaferro@unisa.it

lsarno@unisa.it guido.pirovano@rse-web.it

Abstract

SPHERA v.9.0.0 (RSE SpA) is a FOSS CFD-SPH research code validated on the following application fields: floods with transport of solid bodies and bed-load transport; fast landslides and their interactions with water reservoirs; sediment removal from water bodies; fuel sloshing tanks. SPHERA is featured by several numerical schemes dealing with: transport of solid bodies in fluid flows; treatment of fixed and mobile solid boundaries; dense granular flows and an erosion criterion. The source and executable codes, the input files and the free numerical chain of SPHERA v.9.0.0 are presented. Some reference validations and applications are also provided. SPHERA is developed and distributed on a GitHub public repository.

PROGRAM SUMMARY

Program title: SPHERA v.9.0.0

Licensing provisions: GNU General Public License 3 (GPL)

Programming language: Fortran 95

Supplementary material: software documentation/guide, 37 tutorials

Journal Reference of previous version: Amicarelli A., R. Albano, D. Mirauda, G. Agate, A. Sole, R. Guandalini; 2015; A Smoothed Particle Hydrodynamics model for 3D solid body transport in free surface flows; *Computers & Fluids*, 116:205–228. DOI 10.1016/j.compfluid.2015.04.018

Does the new version supersede the previous version?: Yes

Reasons for the new version: scheme for dense granular flows (i.e. bed-load transport, fast landslides); reference Journal publication: Amicarelli A., B. Kocak, S. Sibilla, J. Grabe; 2017; A 3D Smoothed Particle Hydrodynamics model for erosional dam-break floods; *International Journal of Computational Fluid Dynamics*, 31(10):413-434; DOI 10.1080/10618562.2017.1422731

Nature of problem (approx. 50-250 words): SPHERA v.9.0.0 has been applied to free-surface and multi-phase flows involving the following application fields: floods (with transport of solid bodies,

1 bed-load transport and a domain spatial coverage up to some hundreds of squared kilometres), fast
2 landslides and wave motion, sediment removal from water reservoirs, fuel sloshing tanks,
3 hydrodynamic lubrication.

4 Solution method (approx. 50-250 words): SPHERA v.9.0.0 is a research FOSS (“Free/Libre and
5 Open-Source Software”) code based on the SPH (“Smoothed Particle Hydrodynamics”) technique,
6 a mesh-less Computational Fluid Dynamics numerical method for free surface and multi-phase
7 flows. The five numerical schemes featuring SPHERA v.9.0.0 deal with: dense granular flows;
8 transport of solid bodies in free surface flows; boundary treatment for both mobile and fixed
9 frontiers; 2D erosion criterion.

10 Additional comments including Restrictions and Unusual features (approx. 50-250 words):
11 SPHERA v.9.0.0 is a 3D research FOSS (“Free/Libre and Open-Source Software”) code (developed
12 under the subversion control system Git) with peculiar features for: floods (with transport of solid
13 bodies, bed-load transport and a domain spatial coverage up to some hundreds of squared
14 kilometres), fast landslides and wave motion, sediment removal from water reservoirs, fuel sloshing
15 tanks, hydrodynamic lubrication. The whole numerical chain of SPHERA is made of FOSS,
16 freeware and Open Data numerical tools.

17 References:

18 SPHERA (RSE SpA), <https://github.com/AndreaAmicarelliRSE/SPHERA>, last access on
19 28May2019

20 Amicarelli A., G. Agate, R. Guandalini; 2013; A 3D Fully Lagrangian Smoothed Particle
21 Hydrodynamics model with both volume and surface discrete elements; International Journal for
22 Numerical Methods in Engineering, 95: 419–450, DOI: 10.1002/nme.4514

23 Amicarelli A., R. Albano, D. Mirauda, G. Agate, A. Sole, R. Guandalini; 2015; A Smoothed
24 Particle Hydrodynamics model for 3D solid body transport in free surface flows; Computers &
25 Fluids, 116:205–228. DOI 10.1016/j.compfluid.2015.04.018

26 Amicarelli A., B. Kocak, S. Sibilla, J. Grabe; 2017; A 3D Smoothed Particle Hydrodynamics model
27 for erosional dam-break floods; International Journal of Computational Fluid Dynamics,
28 31(10):413-434; DOI 10.1080/10618562.2017.1422731

29 Manenti S., S. Sibilla, M. Gallati, G. Agate, R. Guandalini; 2012; SPH Simulation of Sediment
30 Flushing Induced by a Rapid Water Flow; Journal of Hydraulic Engineering ASCE 138(3): 227-
31 311.

32 Di Monaco A., S. Manenti, M. Gallati, S. Sibilla, G. Agate, R. Guandalini; 2011; SPH modeling of
33 solid boundaries through a semi-analytic approach. Engineering Applications of Computational
34 Fluid Mechanics, 5(1):1-15.

35
36
37
38
39
40
41
42 **Keywords.**

43 SPH; FOSS; github; floods; landslides; sediments; transport of solid bodies; erosion; bed-load
44 transport; sloshing tanks; wave motion; dams; boundary treatment methods; dense granular flows;
45 SPHERA; hydrodynamic lubrication.
46
47
48
49
50
51
52
53
54
55
56
57
58
59
60
61
62
63
64
65

1. INTRODUCTION

SPHERA v.9.0.0 (RSE SpA, 2018, [49]) is a research FOSS (“Free/Libre and Open-Source Software”, Free Software Foundation, [21]) code based on the SPH (“Smoothed Particle Hydrodynamics”) technique, a mesh-less Computational Fluid Dynamics method for free surface and multi-phase flows. SPHERA has been applied to floods (with transport of solid bodies, bed-load transport and a domain spatial coverage up to some hundreds of squared kilometres), fast landslides and wave motion, sediment removal from water reservoirs, sloshing tanks.

The main numerical developments featuring SPHERA v.9.0.0 are listed hereafter:

- scheme for dense granular flows (Amicarelli et al., 2017, [7]);
- scheme for the transport of solid bodies in free surface flows (Amicarelli et al., 2015, [6]);
- scheme for a boundary treatment (“DB-SPH” for simplicity of notation) based on discrete surface and volume elements, and on a 1D Linearized Partial Riemann Solver coupled with a MUSCL (Monotonic Upstream-Centered Scheme for Conservation Laws) spatial reconstruction scheme (Amicarelli et al., 2013, [5]);
- scheme for a 2D erosion criterion (Manenti et al., 2012, [35]);
- scheme for a boundary treatment (“semi-analytic approach or SA-SPH” for simplicity of notation) based on volume integrals, numerically computed outside of the fluid domain (Di Monaco et al., 2011, [18]).

Other major numerical developments are available in SPHERA v.9.0.0 in a preliminary form and deal with the following topics: 2-interface 3D erosion criterion; 3D rotations of solid bodies based on Rodrigues formula; sliding friction force; body-boundary normal reaction forces under sliding; soil liquefaction; shear-stress boundary terms for the DB-SPH scheme; damage scheme for electrical substations; pressure limiters for fluid-structure interactions; bottom drag exerted on the fluid; higher order Runge-Kutta time integration schemes; shear stress gradient terms for laminar flows and fluid-structure interactions under no-slip conditions.

SPHERA has been developed for RSE SpA by the following authors (list of the code authors, SPHERA, 2018, [49]): Andrea Amicarelli, Antonio Di Monaco, Sauro Manenti, Elia Giuseppe Bon, Daria Gatti, Giordano Agate, Stefano Falappi, Barbara Flamini, Roberto Guandalini, David Zuccalà, Qiao Cheng. SPHERA is free software released under the GNU General Public License (Free Software Foundation) and its Copyright is registered at SIAE. SPHERA is indexed by SPHERIC ([50]).

SPHERA is based on the SPH technique, whose basic features are briefly recalled hereafter.

Smoothed Particle Hydrodynamics (SPH) is a mesh-less CFD method, whose computational nodes are represented by numerical fluid particles. In the continuum, the functions and derivatives in the fluid dynamics balance equations are approximated by convolution integrals, which are weighted by interpolating (or smoothing) functions, called kernel functions.

The integral SPH approximation ($\langle \cdot \rangle_I$) of a generic function (f) is defined as:

$$\langle f \rangle_{I, \underline{x}_0} = \int_{V_h} f W dx^3 \quad (1.1)$$

where W (m^{-3}) is the kernel function (Monaghan, 2005, [38]), \underline{x}_0 (m) is the position of a generic computational point and V_h (m^3) is the integration volume, which is called kernel support. This is represented by a sphere of radius $2h$ (m), where h is a characteristic length of the kernel support, which is possibly truncated by the frontiers of the fluid domain.

Any first derivative of a generic function, calculated along i -axis, can be computed as in (1.1), after replacing f with the targeted derivative. After integration by parts, one obtains:

$$\left\langle \frac{\partial f}{\partial x_i} \right\rangle_{I, \underline{x}_0} = \int_{A_h} f W n_i dx^2 - \int_{V_h} f \frac{\partial W}{\partial x_i} dx^3 \quad (1.2)$$

The integration also involves the surface A_h (m^2) of the kernel support whose local orientation is defined by the normal \underline{n} . The associated surface integral is non-zero in case of a truncated kernel support. The representation of this term noticeably differentiates the various SPH codes developed by the research community (Adami et al., 2012, [2]; Hashemi et al., 2012, [27]; Macia et al., 2012, [33]; Mayrhofer et al., 2013, [37]; Ferrand et al., 2013, [20]; Amicarelli et al., 2013, [5]).

1
2
3
4
5
6
7
8
9
10
11
12
13
14
15
16
17
18
19
20
21
22
23
24
25
26
27
28
29
30
31
32
33
34
35
36
37
38
39
40
41
42
43
44
45
46
47
48
49
50
51
52
53
54
55
56
57
58
59
60
61
62
63
64
65

Far from boundaries, the SPH particle approximation of (1.2) reads:

$$\left\langle \frac{\partial f}{\partial x_i} \right\rangle_{x_0} = - \sum_b f_b \frac{\partial W}{\partial x_i} \Big|_b \omega_b \quad (1.3)$$

where a summation on particle volumes ω (m³) replaces the volume integral. The subscripts “ θ ” and “ b ” refer to the computational particle and its “neighbouring particles” (fluid particles within the kernel support of the computational particle), respectively. Each particle represents a mobile fluid volume featured by the fluid dynamics physical quantities and a time-dependent position. In order to minimize the SPH truncation errors, initial conditions define any particle volume as a cube and any particle position as coincident with the associated particle volume barycentre. There is no need to define the time evolution of the edges and the barycentre of the SPH particle volumes. More details on the SPH particle discretization are available in Monaghan (2005, [38]).

Usually, the approximation (1.3) is replaced by more complicated and accurate formulas. Further, the SPH method can also approximate a generic n-th derivative, analogously to (1.3).

Among the various numerical methods, Smoothed Particle Hydrodynamics (SPH) has several advantages: a direct estimation of free surface and phase/fluid interfaces; effective simulations of multiple moving bodies and particulate matter within fluid flows; direct estimation of Lagrangian derivatives (absence of non-linear advective terms in the balance equations); effective numerical simulation of fast transient phenomena; no meshing; simple non-iterative algorithms (in case the “Weakly Compressible” approach is adopted). On the other hand, SPH models are affected by the following drawbacks, if compared with mesh-based CFD tools: computational costs are slightly higher due to a larger stencil (around each computational particle), which causes a high number of interacting elements (neighbouring particles) at a fixed time step (nonetheless SPH codes are more suitable to parallelization); local refining of spatial resolution represents a current issue and is only addressed by few advanced and complex SPH algorithms; accuracy is relatively low for classical CFD applications where mesh-based methods are well established (e.g., confined mono-phase flows). Detailed reviews on SPH assets and drawbacks have been reported in Gomez-Gesteira et al.

1 (2010, [24]), Le Touzé et al. (2013, [31]), Shadloo et al. (2016, [48]),Violeau and Rogers (2016,
2 [59]). Nevertheless, SPH models are effective in several, but peculiar, application fields. Some of
3 them are herein briefly recalled: flood propagation (e.g., Gu et al., 2017, [26]; Vacondio et al.,
4 2012, [54]; Crespo et al., 2008, [17]); sloshing tanks (e.g., Khayyer et al., 2018, [29] ; Amicarelli et
5 al., 2013, [5]); gravitational surface waves (e.g. Colagrossi et al., 2013, [13]; Crespo et al., 2007,
6 [15]) and marine energy converters (Crespo et al., 2017, [14]); hydraulic turbines (e.g., Marongiu et
7 al., 2010, [36]); liquid jets (e.g., Marongiu et al., 2010, [36]); astrophysics and magneto-
8 hydrodynamics (e.g., Price, 2012, [43]); body dynamics in free surface flows (e.g., Amicarelli et al.,
9 2015, [6]); multi-phase and multi-fluid flows; sediment removal from water reservoirs (e.g.,
10 Manenti et al., 2012, [35]); landslides (e.g., Abdelrazek et al., 2016, [1]; Bui et al., 2008, [11]).
11 Some advanced multi-purpose SPH codes are available as FOSS (e.g., Crespo et al., 2015, [16]).
12
13
14
15
16
17
18
19
20
21
22
23
24
25
26
27
28
29
30
31
32
33
34
35
36
37
38
39
40
41
42
43
44
45
46
47
48
49
50
51
52
53
54
55
56
57
58
59
60
61
62
63
64
65

2. SCHEME FOR TRANSPORT OF SOLID BODIES AND THE SEMI-ANALYTIC APPROACH AS A BOUNDARY TREATMENT SCHEME FOR FIXED BOUNDARIES

This section describes the balance equations for fluid (Sec.2.1) and body (Sec.2.2) dynamics, the 2-way interaction terms related to both fluid-body (Sec.2.3) and solid-solid (Sec.2.4) interactions, the semi-analytic approach for treating fixed boundaries (Sec.2.1).

2.1. SPH approximation of the balance equations for fluid dynamics and the boundary treatment scheme called “semi-analytic approach”

The numerical scheme for the main flow is a Weakly-Compressible (WC) SPH model, which takes benefit from a boundary treatment for fixed boundaries based on the semi-analytic approach of Vila (1999, [57]), as developed by Di Monaco et al. (2011, [18]).

One considers Euler’s momentum and continuity equations:

$$\begin{aligned} \frac{du_i}{dt} &= -\frac{1}{\rho} \frac{\partial p}{\partial x_i} - \delta_{i3} g, \quad i = 1,2,3 \\ \frac{d\rho}{dt} &= -\rho \nabla \cdot \underline{u} \end{aligned} \tag{2.1}$$

where $\underline{u} \equiv (u, v, w)$ (m/s) is the velocity vector, p (Pa) is the pressure, ρ (kg/m³) is the fluid density, δ_{ij} is Kronecker’s delta function and t (s) denotes time. One needs to compute (2.1) at each fluid particle position by using the SPH formalism and by taking into account the boundary terms (fluid-frontier and fluid-body interactions), as described below.

One considers the discretization of (2.1), as provided by the SPH approximation of the first derivative of a generic function (f) -a variant of (1.3)-, according to the semi-analytic approach (“SA”; Vila, 1999, [57]):

$$\left\langle \frac{\partial f}{\partial x_i} \right\rangle_{SA,0} = -\sum_b (f_b - f_0) \frac{\partial W_b}{\partial x_i} \omega_b - \int_{V'_n} (f - f_0) \frac{\partial W}{\partial x_i} dx^3 \tag{2.2}$$

The inner fluid domain here involved is filled with numerical particles. At boundaries, the kernel support is (formally) not truncated because it can partially lie outside the fluid domain. In other words, the summation in (2.2) is performed over all the fluid particles “ b ” (neighbouring particles

with volume ω) in the kernel support of the computational fluid particle (“ ϕ ”). At the same time, the volume integral in (2.2) represents the boundary term, which is a convolution integral on the truncated portion of the kernel support. In this fictitious and outer volume V_h' (m^3), one needs to define the generic function f (pressure, velocity or density alternatively).

The semi-analytic approach (“ $_{SA}$ ”) (as developed by Di Monaco et al., 2011, [18]) introduces the following linearization and assumptions to compute f in V_h' :

$$\left\langle \frac{\partial f}{\partial x_i} \right\rangle_{SA} = -\sum_b (f_b - f_0) \frac{\partial W_b}{\partial x_i} \omega_b - \int_{V_h'} (f_{SA} - f_0) \frac{\partial W}{\partial x_i} dx^3 - \int_{V_h'} \frac{\partial f}{\partial x_i} \Big|_{SA} (\underline{x} - \underline{x}_0) \frac{\partial W}{\partial x_i} dx^3 \quad (2.3)$$

The peculiar “ $_{SA}$ ” values of the functions and derivatives within V_h' are assigned to represent a null normal gradient of reduced pressure at the frontier interface (while considering uniform density):

$$p_{SA} = p_0, \quad \left\langle \frac{\partial p}{\partial x_i} \right\rangle_{SA} = -\delta_{i3} \mathbf{g}; \quad \rho_{SA} = \rho_0, \quad \left\langle \frac{\partial \rho}{\partial x_i} \right\rangle_{SA} = 0 \quad (2.4)$$

At the same time, the model sets free-slip conditions when estimating velocity at boundaries. The velocity vector is taken as uniform in the outer part of the kernel support. Here \underline{u}_{SA} is decomposed into the sum of a vector normal to boundary ($\underline{u}_{SA,n}$) and a tangential vector ($\underline{u}_{SA,T}$). The first is represented as a linear extrapolation from the computational fluid particle velocity. The latter is equal to its analogous vector of the same computational fluid particle (the subscript “ $_w$ ” refers to a generic frontier), in case of free-slip conditions:

$$\left. \begin{aligned} \underline{u}_{SA} &= \underline{u}_{SA,T} + \underline{u}_{SA,n} = \underline{u}_{0,T} + \left[(2\underline{u}_w - \underline{u}_0) \cdot \underline{n} \right] \underline{n} \\ \underline{u}_{SA,T} &= \underline{u}_{0,T}, \quad \left\langle \frac{\partial u_i}{\partial x_i} \right\rangle_{SA} = 0 \end{aligned} \right\} \Rightarrow \underline{u} - \underline{u}_0 = \underline{u}_{SA} - \underline{u}_0 = 2 \left[(\underline{u}_w - \underline{u}_0) \cdot \underline{n} \right] \underline{n} \quad (2.5)$$

where \underline{n} is the normal vector of the wall surface, as defined by its local orientation.

At this point, one can write the continuity equation for a Weakly Compressible SPH model (Einstein’s notation is herein adopted for the subscript “ $_j$ ”), using the semi-analytic approach for the boundary integral term (second term on the Right Hand Side):

$$\left\langle \frac{d\rho}{dt} \right\rangle_0 = \sum_b \rho_b (\underline{u}_{b,j} - \underline{u}_{0,j}) \frac{\partial W}{\partial x_j} \Big|_b \omega_b + 2\rho_0 \int_{V_h} [(\underline{u}_w - \underline{u}_0) \cdot \underline{n}] n_j \frac{\partial W}{\partial x_j} dx^3 + C_s \quad (2.6)$$

where C_s ($\text{kg} \times \text{m}^{-3} \times \text{s}^{-1}$) is introduced to represent a fluid-body interaction term.

On the other hand, one can analogously derive the approximation of the momentum equation (the notation $\langle \rangle$ indicates the SPH particle -discrete- approximation):

$$\begin{aligned} \left\langle \frac{d\underline{u}_i}{dt} \right\rangle_0 &= -\delta_{i3} \underline{g} + \sum_b \left(\frac{p_b}{\rho_b^2} + \frac{p_0}{\rho_0^2} \right) \frac{\partial W}{\partial x_i} \Big|_b m_b + \\ &+ 2 \frac{p_0}{\rho_0} \int_{V_h} \frac{\partial W}{\partial x_i} dx^3 + -\nu_M \sum_b \frac{m_b}{\rho_0 r_{0b}^2} (\underline{u}_b - \underline{u}_0) \cdot (\underline{x}_b - \underline{x}_0) \frac{\partial W}{\partial x_i} \Big|_b + \\ &- 2\nu_M (\underline{u}_w - \underline{u}_0) \cdot \int_{V_h} \frac{1}{r_{0w}^2} (\underline{x} - \underline{x}_0) \frac{\partial W}{\partial x_i} \Big|_b dx^3 + \underline{a}_s + 2\nu_0 (\underline{u}_w - \underline{u}_0) \int_{V_h} \frac{1}{r} \left| \frac{\partial W}{\partial r} \right|_b dx^3 \end{aligned} \quad (2.7)$$

where \underline{a}_s ($\text{m} \times \text{s}^{-2}$) represents a new acceleration term due to the fluid-body interactions, ν_M ($\text{m}^2 \times \text{s}^{-1}$) is the artificial viscosity (Monaghan, 2005, [38]), m (kg) is the particle mass and r (m) is the relative distance between the neighbouring and the computational particle.

Finally, a barotropic equation of state (EOS) is linearized as follows:

$$p \cong c_{ref}^2 (\rho - \rho_{ref}) \quad (2.8)$$

The artificial sound speed c (m/s) is 10 times higher than the maximum fluid velocity (WC approach) and “ $_{ref}$ ” stands for a reference state.

More details are available in Amicarelli et al. (2015, [6]) and Di Monaco et al. (2011, [18]).

2.2. SPH balance equations for rigid body transport

Body dynamics is ruled by Euler-Newton equations, whose discretization takes advantage from the SPH formalism and the coupling terms derived in the following sections:

$$\begin{aligned} \frac{d\underline{u}_{CM}}{dt} &= \frac{\underline{F}_{TOT}}{m_B}, & \frac{d\underline{x}_{CM}}{dt} &= \underline{u}_{CM} \\ \frac{d\underline{\chi}_B}{dt} &= \underline{I}_C^{-1} \left[\underline{M}_{TOT} - \underline{\chi}_B \times \left(\underline{I}_C \underline{\chi}_B \right) \right] & \frac{d\underline{\alpha}}{dt} &= \underline{\chi}_B \end{aligned} \quad (2.9)$$

Here the subscript “ B ” refers to a generic computational body and “ CM ” to its centre of mass. The first two formulas of (2.9) represent the balance equations for the momentum and the time law for the position of the body barycentre \underline{F}_{TOT} ($\text{kg}\times\text{m}\times\text{s}^{-2}$) being the global/resultant force exerted on the solid-. The last two formulas of (2.9) express the balance equation of the angular momentum $\underline{\omega}^B$ ($\text{rad}\times\text{s}^{-1}$) denotes the angular velocity of the generic body- and the time evolution of the solid orientation $\underline{\alpha}$ (rad) is the vector of Euler angles lying between the body axes and the global reference system-. \underline{M}_{TOT} ($\text{kg}\times\text{m}^2\times\text{s}^{-2}$) represents the associated torque acting on the body and \underline{I}_C ($\text{kg}\times\text{m}^2$) the matrix of the moments of inertia of the computational body (Einstein’s notation applied for the subscript “ i ”):

$$I_{c,ij} = \int_{V_B} \rho (r_l^2 \delta_{ij} - r_i r_j) dV = \begin{cases} \int_{V_B} \rho (r_k^2 + r_n^2) dV, i = j; k, n \neq i \\ - \int_{V_B} \rho (r_i r_j) dV, i \neq j \end{cases} \quad (2.10)$$

In this sub-section, \underline{r} implicitly represents the relative distance from the body centre of mass.

In order to solve the system (2.9), we need to model the global force and torque, as described in the following.

The resultant force is composed of several terms:

$$\underline{F}_{TOT} = \underline{G} + \underline{P}_F + \underline{T}_F + \underline{P}_S + \underline{T}_S, \quad \underline{T}_F + \underline{T}_S \cong \underline{0} \quad (2.11)$$

where \underline{G} ($\text{kg}\times\text{m}\times\text{s}^{-2}$) represents the gravity force, whereas \underline{P}_F ($\text{kg}\times\text{m}\times\text{s}^{-2}$) and \underline{T}_F ($\text{kg}\times\text{m}\times\text{s}^{-2}$) the vector sums of the pressure and shear forces provided by the fluid. Analogously, \underline{P}_S ($\text{kg}\times\text{m}\times\text{s}^{-2}$) and \underline{T}_S ($\text{kg}\times\text{m}\times\text{s}^{-2}$) are the vector sums of the normal and the shear forces provided by other bodies or boundaries (solid-solid interactions). In case of inertial and quasi-inertial fluid flows, we do not need to refer to neither turbulence scheme nor tangential stresses (simplifying hypothesis).

The fluid-solid interaction is expressed by the hydrodynamic thrust:

$$\underline{P}_F = \sum_s p_s A_s \underline{n}_s \quad (2.12)$$

1 The computational body is numerically represented by solid volume elements, here called (solid)
 2 “body particles” (“ s ”). Some of them describe the body surface and are referred to as “surface body
 3 particles”. These particular elements are also characterized by an area and a vector \underline{n} of norm 1.
 4 This is perpendicular to the body face of the particle (it belongs to) and points outward the fluid
 5 domain (inward the solid body). Graphical and in-depth details are available in Amicarelli et al.
 6 (2015, [6]).

7 The pressure of a body particle is computed as described in Sec.2.3, whereas the treatment of the
 8 solid-solid interaction term (\underline{P}_s) is discussed in Sec.2.4.

9 The torque in (2.9) is discretized as the summation of each vector product between the relative
 10 position \underline{r}_s , of a surface body particle with respect to the body centre of mass, and the corresponding
 11 total particle force:

$$12 \quad \underline{M}_{TOT} = \sum_s \underline{r}_s \times \underline{F}_s \quad (2.13)$$

13 Time integration of (2.9) is performed using a Leapfrog scheme synchronized with the fluid
 14 dynamics balance equations. This means that the body particle pressure is computed simultaneously
 15 to the fluid pressure, so that this parameter is staggered of around $dt/2$ (s) with respect to all the
 16 other body particle parameters.

17 After time integration, the model obtains the velocity of a body particle as the vector sum of the
 18 velocity of the corresponding body barycentre and the relative velocity:

$$19 \quad \underline{u}_s = \underline{u}_{CM} + \underline{\chi}_B \times \underline{r}_s \quad (2.14)$$

20 Finally, the model updates the body particle normal vectors and absolute positions, according to the
 21 following kinematics formulas - $d\alpha$ (rad) is the vector increment in Euler’s angles during the current
 22 time step and R_{ij} is the body rotation matrix-:

$$23 \quad \underline{n}_s(t+dt) = \underline{R}_B \underline{n}_s(t), \quad \underline{x}_s(t+dt) = \underline{x}_{CM}(t+dt) + \underline{R}_B \underline{r}_s(t) \quad (2.15)$$

$$24 \quad \underline{R}_B = \underline{R}_x \underline{R}_y \underline{R}_z, \quad d\alpha_B = \underline{\chi}_B dt$$

$$\underline{\underline{R}}_x = \begin{bmatrix} 1 & 0 & 0 \\ 0 & \cos(d\alpha_x) & -\sin(d\alpha_x) \\ 0 & \sin(d\alpha_x) & \cos(d\alpha_x) \end{bmatrix}, \underline{\underline{R}}_y = \begin{bmatrix} \cos(d\alpha_y) & 0 & \sin(d\alpha_y) \\ 0 & 1 & 0 \\ -\sin(d\alpha_y) & 0 & \cos(d\alpha_y) \end{bmatrix}, \underline{\underline{R}}_z = \begin{bmatrix} \cos(d\alpha_z) & -\sin(d\alpha_z) & 0 \\ \sin(d\alpha_z) & \cos(d\alpha_z) & 0 \\ 0 & 0 & 1 \end{bmatrix}$$

More details are available in Amicarelli et al. (2015, [6]).

2.3. Fluid-body interaction terms

The fluid-body interaction terms rely on the boundary technique introduced by Adami et al. (2012, [2]), as implemented and adapted for free-slip conditions by Amicarelli et al. (2015, [6]). If boundary is fixed, this method can be interpreted as a discretization of the semi-analytic approach used to treat fluid-boundary interactions (Sec.2.1). The outer domain of (2.2) is herein represented by all the body particles inside the kernel support of the computational fluid particle. Further, Adami et al. (2012, [2]) introduced a new term, related to the acceleration of the fluid-solid interface, which influences the estimation of body particle pressure.

The fluid-body interaction term in the continuity equation represents a discrete approximation of the analogous term in (2.6), used to treat solid frontiers (free-slip conditions):

$$C_s = 2\rho_0 \sum_s [(\underline{u}_s - \underline{u}_0) \cdot \underline{n}_s] W'_s \omega_s \quad (2.16)$$

Analogously, the fluid-body interaction term in the momentum equation (2.7) assumes the form:

$$\underline{a}_s = \sum_s \left(\frac{p_s + p_0}{\rho_0^2} \right) W'_s m_s \quad (2.17)$$

The pressure value of the generic neighbouring surface body particle “s” depends on the particular computational fluid particle “o” we are considering, so that we can refer to the interaction subscript “s,o”. One may apply a SPH interpolation over all the pressure values coming from fluid-body particle interactions to derive a unique pressure value for each body particle (no-slip conditions):

$$p_s = \frac{\sum_0 \left\{ p_0 + \rho_0 [(\underline{g} - \underline{a}_s) \cdot \underline{n}_w] [(\underline{x}_s - \underline{x}_0) \cdot \underline{n}_w] \right\} W_{0s} \left(\frac{m_0}{\rho_0} \right)}{\sum_0 W_{0s} \left(\frac{m_0}{\rho_0} \right)} \quad (2.18)$$

More details are available in Amicarelli et al. (2015, [6]).

2.4. Solid-solid interaction terms

The solid-solid interaction term \underline{P}_s in (2.11) represents body-body and body-boundary impingement forces, whose time and spatial evolution, in the continuum, is theoretically proportional to Dirac's delta function. The numerical model needs to discretize \underline{P}_s , as explained hereafter.

The “boundary force particle” method of Monaghan (2005, [38]) defines repulsive forces to represent a conservative full elastic impingement between two SPH interacting particles (of any medium), conserving both global momentum and kinetic energy. The formulation above applies for inter-particle high velocity impacts and is implemented and extended to whole solid bodies (not only particle impingements), even at low velocities, as well as body-frontier interactions (Amicarelli et al., 2015, [6]).

One considers the overall force \underline{P}_s , which represents the impingements between a generic computational body (“ B ”) and all its neighbouring bodies (“ K ”) and frontiers (“ K^* ”). \underline{P}_s is decomposed in elementary 2-body (\underline{P}_{BK}) and body-frontier (\underline{P}_{BK^*}) interactions:

$$\underline{P}_s = \sum_K \underline{P}_{BK} + \sum_{K^*} \underline{P}_{BK^*} \quad (2.19)$$

Invoking the same principles of the boundary force particle method, \underline{P}_{BK} involves interactions between all the body particles “ j ” of the computational body “ B ” and their neighbour body particles “ k ”, belonging to the neighbouring body “ K ”:

$$\underline{P}_{BK} = -\alpha_I \sum_j \sum_k \frac{2u_{\perp,jk}^2}{r_{per,jk}} \frac{m_j m_k}{m_j + m_k} \Gamma_{jk} \left(1 - \frac{r_{par,jk}}{dx_s} \right) \underline{n}_k \quad (2.20)$$

The components of the inter-particle relative distance, r_{par} and r_{per} , are parallel and perpendicular to the neighbour normal, respectively. The term within brackets in (2.20) deforms the kernel support of the body particles “ j ”, so that it mainly develops along the direction aligned with the normal of the neighbouring particle $-dx_s$ (m) is the size of the solid body particles-. The weighting function Γ is expressed according to Monaghan (2005, [38]) and depends on $q = r_{jk}/h$:

$$\Gamma_{jk} = \begin{cases} \frac{2}{3}, & 0 \leq q < \frac{2}{3} \\ \left(2q - \frac{3}{2}q^2\right), & \frac{2}{3} \leq q < 1 \\ \frac{1}{2}(2-q)^2, & 1 \leq q < 2 \\ 0, & 2 \leq q \end{cases} \quad (2.21)$$

SPHERA holds two modifications for body-body interactions, with respect to the original formulation of the boundary force particles. The first one concerns the impact velocity $u_{\perp,jk}$ (m/s), which replaces the term “0.1c” in the formulation of Monaghan (2005, [38]) and properly deals with low velocity impacts. It avoids too strong or too weak impingement forces. For each body-body interaction, the impact velocity has a unique value for all the particle-particle interactions during the on-going time step. This velocity is computed as the maximum of the absolute values of the inter-particle relative velocity (projected over the normal of the neighbouring particle). For this purpose, the scheme considers all the inter-particle interactions recorded while the 2 bodies are approaching. The expression for the impact velocity reads:

$$u_{\perp,jk}(t) = \max_{j,k,t^*} \left\{ \left| (\underline{u}_j - \underline{u}_k) \cdot \underline{n}_k \right| \right\} \quad t_0 \leq t^* \leq t \quad (2.22)$$

where t_0 (s) refers to the beginning of the approaching phase. When other forces (e.g. pressure and gravity forces) are taken into account, the impact velocity can eventually increase in the inter-body impact zone, causing a potential and partial penetration of a solid into another body. Under these conditions, and only during the approaching phase, (2.22) allows increasing the magnitude of the impingement force, depending on the actual impact velocity (instead of the undisturbed impact velocity). This modification avoids mass penetrations in case of complex impingements.

Further, (2.20) introduces the normalizing parameter α_I , which corrects discretization errors and better preserves the global momentum and kinetic energy of the body-body system during the impingement. If one omits α_I , then (2.20) would drastically under-estimate the impingement forces

if the whole mass of the bodies does not lie within the impact zone (of depth $2h$). The expression for α_I assumes the following form:

$$\alpha_I = \frac{1}{r_{per,BK}} \frac{m_B m_K}{m_B + m_K} \Gamma_{BK} \Bigg/ \sum_j \sum_k \left[\frac{1}{r_{per,jk}} \frac{m_j m_k}{m_j + m_k} \Gamma_{jk} \left(1 - \frac{r_{par,jk}}{dx_s} \right) \right] \quad (2.23)$$

where the body impact velocity is represented as a weighted average of the particle impact velocities. As a first approximation, the normalizing factor α_I roughly represents the inverse of the fraction of the system mass which lies into the impingement zone. This mass should numerically represent the whole 2-body system during the impact.

Finally, the model represents body-boundary interactions. A generic boundary is modelled as a body with infinite mass and discretization tending to zero (the semi-analytic approach, used to model frontiers, is an integral method). The interaction force assumes the following expression (here the subscript “ K^* ” refers to a generic neighbouring frontier):

$$\underline{P}_{BK^*} = -\alpha_I \sum_j \frac{2u_{\perp,jK^*}^2}{r_{per,jK^*}} m_j \Gamma_{jK^*} \underline{n}_{K^*}, \quad \alpha_I = \frac{m_B}{r_{per,BK^*}} \Gamma_{BK^*} \Bigg/ \sum_j \left(\frac{m_j}{r_{per,jK^*}} \Gamma_{jK^*} \right) \quad (2.24)$$

More details are available in Amicarelli et al. (2015, [6]).

3. SCHEME FOR DENSE GRANULAR FLOWS

This section describes the mathematical and numerical models of the scheme for dense granular flows (Amicarelli et al., 2017, [7]; Sec.3.1). This mixture model for bed-load transport and fast landslides is consistent with the “packing limit” of the Kinetic Theory of Granular Flow (KTGF, Armstrong et al., 2010, [8]) and no tuning parameter is used to represent the mixture viscosity. In case erosion is the only cause of mobilization of the solid grains, the model above can be possibly sped-up in 2D by means of an erosion scheme (Manenti et al., 2012, [35]; Sec.3.2).

3.1. Mixture model for dense granular flows

This SPH scheme represents the mixture of fluid phase and non-cohesive solid granular material, under the “packing limit” of the Kinetic Theory of Granular Flow (KTGF, Armstrong et al., 2010, [8]) for dense granular flows. This limit refers to the maximum values of the solid phase volume fraction and is peculiar of bed-load transport (e.g., erosional dam breaks) and fast landslides.

Adopting a Weakly Compressible approach, the continuity equation for the mixture reads:

$$\frac{d\rho}{dt} = -\rho \frac{\partial u_j}{\partial x_j} \quad (3.1)$$

The mixture density and velocity (the subscript “*m*” for the mixture quantities are omitted for simplicity of notation) are defined as follows:

$$\rho \equiv \rho_f \varepsilon_f + \rho_s \varepsilon_s, \quad u_i \equiv \frac{\rho_f \varepsilon_f u_{f,i} + \rho_s \varepsilon_s u_{s,i}}{\rho}, \quad i = 1,3 \quad (3.2)$$

The volume fractions (ε) of the fluid (“*f*”) and the solid (“*s*”) phases are constrained to the volume balance equation:

$$\varepsilon_s + \varepsilon_f = 1 \quad (3.3)$$

The model assumes that SPH particles are conservative (i.e. mixture particles do not exchange net mass fluxes with the surrounding environment), which is a reasonable hypothesis for high solid volume fractions in saturated soils, according to the “packing limit” of the Kinetic Theory of Granular Flow (Armstrong et al., 2010, [8]).

Following the multi-phase approach of Colagrossi and Landrini (2003, [12]), the SPH approximation of (3.1) can be expressed as follows:

$$\frac{d\rho_0}{dt} = \rho_0 \sum_b (u_{b,j} - u_{0,j}) \frac{\partial W}{\partial x_j} \Big|_b \omega_b + 2\rho_0 \int_{V_h} [(\underline{u}_w - \underline{u}_0) \cdot \underline{n}] n_j \frac{\partial W}{\partial x_j} dx^3 \quad (3.4)$$

The integral boundary term in (3.4) is computed according to Di Monaco et al. (2011, [18]) and represents the effects of wall frontiers.

The form of the momentum equations for the mixture is identical to Navier-Stokes equations:

$$\frac{du_i}{dt} = -\delta_{i3}g - \frac{1}{\rho} \frac{\partial p}{\partial x_i} + \nu \frac{\partial^2 u_i}{\partial x_j^2} \quad (3.5)$$

where p (Pa) is the mixture total pressure/stress and ν ($\text{m}^2 \times \text{s}^{-1}$) is the mixture kinematic viscosity.

The total stress is computed by means of a barotropic equation of state, formally identical to (2.8).

A unique speed of sound can be chosen (i.e. the highest among the SPH particle values, no matter about their phase volume fractions).

The mixture dynamic viscosity ($\mu \equiv \nu\rho$) ($\text{Pa} \times \text{s}$) is defined as:

$$\mu \equiv \varepsilon_f \mu_f + H(\varepsilon_s - \varepsilon_{s,p}) \mu_{fr} \quad (3.6)$$

where H is the Heaviside step function.

In the ‘‘packing limit’’ of the KTGF (i.e. for ε_s close enough to the value of $\varepsilon_{s,p} = \text{ca.} 0.59$, which is the maximum attainable solid volume fraction for a sheared inelastic hard sphere fluid (Kumaran, 2015, [30]), the shear stress gradient term is represented by means of a visco-plastic model for dry granular material based on internal friction (Schaeffer, 1987, [47]), by means of a physical quantity named frictional viscosity μ_{fr} ($\text{Pa} \times \text{s}$):

$$\mu_{fr} \equiv \left(\frac{\sigma'_m (\sin \varphi)}{2\sqrt{I_2(e_{ij})}} \right) \quad (3.7)$$

Here φ (rad) is the internal friction angle, e_{ij} (s^{-1}) the strain-rate tensor and $I_2(e_{ij})$ (s^{-2}) is its second invariant (formulation for incompressible fluids):

$$e_{ij} \equiv \frac{1}{2} \left(\frac{\partial u_i}{\partial x_j} + \frac{\partial u_j}{\partial x_i} \right), |e_{ij}| \equiv \left(\sum_{i,j} e_{ij}^2 \right)^{\frac{1}{2}} = \sqrt{2I_2(e_{ij})} \quad (3.8)$$

The mean effective stress σ'_m (Pa) is computed as the difference between the total stress and the fluid pressure, according to the principle of Terzaghi (1943, [53]):

$$p = p_f + \sigma'_m \quad (3.9)$$

The fluid pressure in the granular material is related to two different soil conditions, as follows:

$$p_f = \begin{cases} p_{f,blt-top} + \rho_f g (z_{blt-top}|_{x_0,y_0} - z_0) \cos^2(\alpha_{TBT}), & \text{fully saturated soil} \\ 0, & \text{dry soil} \end{cases} \quad (3.10)$$

where the subscript “ $_{blt-top}$ ” refers to the top of the bed-load transport layer (or the layer of saturated material). Eq.(3.10) assumes a 1D filtration flow parallel to the slope of the granular material. This simplifying hypothesis is still consistent with SPH conservative particles; α_{TBT} (rad) is the topographic angle at the top of the bed-load transport layer and lies between the local interface normal and the vertical.

Following the multi-phase approach of Colagrossi and Landrini (2003, [12]), with the boundary treatment method proposed by Di Monaco et al. (2011, [18]), the SPH approximation of the momentum equations (3.5) becomes:

$$\left\langle \frac{du_i}{dt} \right\rangle_0 = -\delta_{i3}g + \frac{1}{\rho_0} \sum_b (p_b + p_0) \frac{\partial W}{\partial x_i} \Big|_b \omega_b + 2 \frac{p_0}{\rho_0 r_h} \int \frac{\partial W}{\partial x_i} \Big|_b dx^3 + 2\nu \sum_b \frac{m_b}{\rho_0 r_{0b}} (\underline{u}_b - \underline{u}_0) \frac{\partial W}{\partial r} \Big|_b + \nu_M \sum_b \frac{m_b}{\rho_0 r_{0b}^2} (\underline{u}_b - \underline{u}_0) \cdot (\underline{x}_b - \underline{x}_0) \frac{\partial W}{\partial x_i} \Big|_b - \nu_M (\underline{u}_{SA} - \underline{u}_0) \cdot \left(\int_{r_{0w}}^1 \frac{1}{r_{0w}^2} (\underline{x} - \underline{x}_0) \frac{\partial W}{\partial x_i} dx^3 \right) \quad (3.11)$$

In order to pinpoint the elasto-plastic regime and avoid the unbounded growth of (3.7), the threshold ν_{max} ($m^2 \times s^{-1}$) for the mixture viscosity is introduced. Mixture particles with a higher viscosity value are considered in the elasto-plastic regime of soil deformation. As their displacements are negligible, these particles are kept fixed as long as they belong to this regime and their pressure is derived from the mixture particles flowing above them. The viscosity threshold is assumed to be high enough not to influence the simulation results.

Further details are available on Amicarelli et al. (2017, [7]).

3.2. 2D erosion criterion

An erosion criterion (Manenti et al., 2012, [35]) is implemented to speed-up the 2D simulations of the scheme for dense granular flows (Sec.3.1), only for those configurations where erosion is the only cause of mobilization of the solid grains. The erosion criterion aims to select those mixture particles, which needs the scheme for dense granular flows (Sec.3.1) to be applied.

The 2D erosion scheme considers the interface “pure fluid - fixed bed” and it is based on the formulation of Shields - van Rijn (1993, [55]). The erosion criterion refers to the interaction of a generic fixed mixture particle and the pure fluid above. Its reference quantities are represented by the closest mobile particle (of pure fluid) above the fixed mixture particle.

The erosion criterion is satisfied if the Shields parameter (θ), which is defined as:

$$\theta \equiv \frac{\tau_*}{g(\rho_s - \rho_f)d_{50}}, \quad \tau_* \equiv \rho_f u_*^2 \quad (3.12)$$

is equal or greater than its critical value θ_c , expressed by van Rijn (1993, [55]):

$$\theta_c = \begin{cases} 0.010595 \ln(\text{Re}_*) + \frac{0.110476}{\text{Re}_*} + 0.0027197, & \text{Re}_* \leq 500 \\ 0.068, & \text{Re}_* > 500 \end{cases} \quad (3.13)$$

Re_* is defined as the grain Reynolds number:

$$\text{Re}_* \equiv \frac{d_{50} u_*}{\nu_f} \quad (3.14)$$

where d_{50} (m) is the 50-th percentile of the particle-size distribution of the soil.

If the height of the liquid particle $z=x_3$ belongs to the Surface Neutral Boundary Layer (SNBL), then the friction velocity u_* (m/s) is iteratively computed according to the similarity theory for the SNBL and the formula for the roughness coefficient z_0 (m) generalized by Manenti et al. (2012, [35]):

$$u_* = \frac{k_v U}{\ln\left(\frac{z}{z_0}\right)}, \quad z_0 = 0.11 \frac{\nu_f}{u_*} + \frac{d_{50}}{30} \quad (3.15)$$

1 where k_v is von Kármán constant and U (m/s) the flow velocity at the height of the liquid particle.

2 If the liquid particle lies below the SNBL, then the model considers the velocity profile of the Sub-
3 Viscous Layer, with the following direct estimation for the friction velocity:
4

$$5 \quad u_* = \sqrt{\frac{Uv_f}{z}} \quad (3.16)$$

6
7
8
9
10 The 2D erosion criterion is derived under 1D stationary and uniform conditions, and does not
11 explicitly depends on the internal friction angle of the granular material.
12

13
14 Graphical and further in-depth details are available on Manenti et al. (2012, [35]).
15
16
17
18
19
20
21
22
23
24
25
26
27
28
29
30
31
32
33
34
35
36
37
38
39
40
41
42
43
44
45
46
47
48
49
50
51
52
53
54
55
56
57
58
59
60
61
62
63
64
65

4. DB-SPH BOUNDARY TREATMENT SCHEME

The activation of the “Discrete Boundary” (DB) - SPH method for boundary treatment (Amicarelli et al., 2013, [5]) allows to treat fixed and mobile solid boundaries and also alters the balance equations in the internal domain of Sec.2.1. The following sub-sections briefly describes the DB-SPH particle approximation (Sec.4.1), the modifications of the balance equations in the inner domain (Sec.4.1) and the 1D Linearized Partial Riemann Solver associated with DB-SPH (Sec. 4.2).

4.1. DB-SPH particle approximation and modifications of the balance equations in the inner domain

According to the DB-SPH method, the first derivative of a generic function (f) is approximated by means of the following SPH particle approximation:

$$\left\langle \frac{\partial f}{\partial x_i} \right\rangle_{\mathbf{x}_0} \equiv \sum_a (f_a) \frac{W_a}{\gamma_0} n_{i,a} \omega_a - \sum_b (f_b) \frac{W'_b}{\gamma_0} \omega_b, \quad W'_b \equiv \frac{\partial W}{\partial x_i} \Big|_b, \quad \gamma \equiv \int_{V_h} W dx^3 \quad (4.1)$$

The volume integral of (1.2) is here replaced with a summation over the fluid particles within the kernel support. The surface integral of (1.2) is herein replaced with a summation over the wall surface elements “ a ” intercepted by the kernel support volume V_h , which is normalized by the integral Shepard coefficient γ . This normalization allows considering the truncated kernel support as if it were entire (in the continuum), but with non-spherical shape. Eq. (4.1) is used to approximate the pressure gradient term of Euler momentum equations (2.1).

The DB-SPH scheme adopts semi-particles, whose 3D definition is slightly different from the edge particles (semi-particles) of Ferrand et al. (2013, [20]). The “semi-particles” represent special fluid particles, which are smallest than the (inner) fluid particles. Each semi-particle is associated to a surface wall element. Semi-particle positions are formally located at the solid frontiers of the fluid domain, but the volumes of the semi-particles completely lie in the inner domain and touch the solid boundaries. The union of the semi-particle volumes represents a thin film of fluid, which is a buffer zone between the inner domain (filled with computational particles) and the wall frontiers. The film depth is smaller than the characteristic length of the fluid particles dx (m).

Surface elements and semi-particles share the same values of their physical quantities. Every surface element is defined by its position, velocity vector, area (length in 2D) and normal vector.

Semi-particles additionally require the mass.

When activating the DB-SPH boundary treatment, a SPH particle approximation of density replaces the continuity equation in the inner domain (Ferrand et al., 2013, [20]):

$$\langle \rho \rangle_0 = \frac{\sum_{bs} \rho_{bs} W_{bs} \omega_{bs}}{\tilde{\gamma}_0} \quad (4.2)$$

where the kernel is normalized by a corrected estimation of the integral Shepard coefficient and the subscript “s” refers to the semi-particles.

The following correction of γ avoids excessive SPH truncation errors at the free surface:

$$\tilde{\gamma} \equiv \begin{cases} \sigma, & \gamma \geq \sigma + \sigma_\varepsilon \\ \gamma, & \gamma < \sigma + \sigma_\varepsilon \end{cases}, \quad \sigma \equiv \sum_{bs} W_{bs} \omega_{bs} \quad (4.3)$$

The integral Shepard coefficient is replaced with the discrete Shepard coefficient at the free surface, which is numerically defined where $\gamma \geq \sigma + \sigma_\varepsilon$. The constant σ_ε can be set equal to 0.05 or chosen as an input parameter to better detect the free surface, depending on the test case and the spatial resolution.

A direct estimation of γ would imply the expensive estimation of 3D analytical integrals. Instead, the present model follows the procedure of Ferrand et al. (2013, [20]), who consider the Lagrangian derivative of γ :

$$\frac{d\gamma}{dt} \cong \sum_a W_a \underline{n}_a \cdot (\underline{u}_a - \underline{u}_0) \omega_a, \quad \frac{\partial W}{\partial t} = 0 \quad (4.4)$$

The initial values of γ are approximately provided by the associated values of σ , as the model exactly assigned the initial values of the fluid particle volumes:

$$\gamma_0(t=0) \equiv \begin{cases} 1, & \min \{r_{0a}\} \geq 2h \\ \sigma_0(t=0), & \min \{r_{0a}\} < 2h \end{cases} \quad (4.5)$$

Further details are available in Amicarelli et al. (2013, [5]).

4.2. 1D Linearized Partial Riemann Solver

At boundaries, the fluid velocity component, which is perpendicular to the wall frontier, is equal to the same component of the frontier velocity (non-penetration condition). The model adopts a 1D LPRS (Linearized Partial Riemann Solver) to impose boundary conditions at the wall elements and semi-particles. The 1D LPRS is an up-wind scheme, also used in SPH-ALE modelling (Marongiu et al., 2010, [36]), which allows wall pressure being approximately compatible with the 3D pressure and velocity fields in the inner domain (constrained to the frontier kinematics).

The definition of the initial conditions (“ L ”, “Left”) of the 1D LPRS are described by means of a first order MUSCL spatial reconstruction scheme. For each interaction (“ $0a$ ”) between a surface element (“ a ”) and a fluid particle (“ ρ ”), the LPRS initial conditions are defined at the position of the wall element. Here the model estimates density and the velocity components, by means of the MUSCL scheme around the computational particle (f alternatively refers to density and every velocity component):

$$f_{0a}^L \cong f_0 + \langle \underline{\nabla f} \rangle_0 \cdot \langle \underline{x}_a - \underline{x}_0 \rangle, \quad u_{n,0a} = \underline{u}_{0a}^L \cdot \underline{n}_a \quad (4.6)$$

The velocity vector is projected along the normal of the surface wall element to obtain \underline{u}_n .

The solution (*) of the LPRS (at the wall element position) provides a reconstructed density value, whereas the associated pressure comes from the equation of state:

$$\rho_{0a}^* = \rho_{0a}^L + (\underline{u}_{n,0a}^L - u_{n,a}) \frac{\rho_{0a}^L}{c_{0a}^L}, \quad p_{0a} = c^2 (\rho_{0a}^* - \rho_0) \quad (4.7)$$

So far, the scheme has estimated several pressure values, at each wall element. The following SPH approximation of these values (summation over all the neighbouring fluid particles) provides a unique pressure value for the surface element:

$$p_a = \frac{\sum_a p_{0a} (W\omega)_a}{\sum_a (W\omega)_a} \quad (4.8)$$

Further details are available in Amicarelli et al. (2013, [5]).

5. TIME INTEGRATION SCHEMES

Time integration is ruled by a second-order Leapfrog scheme (stability analysis and time integration schemes in SPH modelling are discussed in Violeau and Leroy, 2014, [58]), as described in Di Monaco et al. (2011, [18]) and Amicarelli et al. (2015, [6]):

$$\begin{aligned}
 x_i \Big|_{t+dt} &= x_i \Big|_t + u_i \Big|_{t+dt/2} dt, & i = 1,2,3 \\
 u_i \Big|_{t+dt/2} &= u_i \Big|_{t-dt/2} + \left\langle \frac{du_i}{dt} \right\rangle \Big|_t dt, & i = 1,2,3 \\
 \rho \Big|_{t+dt} &= \rho \Big|_t + \left\langle \frac{d\rho}{dt} \right\rangle \Big|_{t+dt/2} dt
 \end{aligned} \tag{5.1}$$

An alternative first-order Runge-Kutta time integration scheme is also available (Euler scheme).

Time integration is constrained by the following stability criteria:

$$dt = \min_0 \left\{ C_v \frac{2h^2}{\nu}; CFL \frac{2h}{c + |\underline{u}|} \right\} \tag{5.2}$$

where CFL is the Courant-Friedrichs-Lewy number. Following Adami et al. (2012, [2]), the viscous term stability parameter is set to $C_v=0.05$.

6. SOURCE CODE, EXECUTABLE CODE, INPUT FILES

A synthetic description of the program units is reported in Sec.6.1; the code compilation and execution are discussed in Sec.6.2; the main input file of SPHERA is presented in Sec.6.3. Further details are available on SPHERA (2018, [49]).

6.1. Synthetic description of the program units

The folders of SPHERA repository are reported in Table 5.1. The program units of SPHERA v.9.0.0 (folder “src”) are grouped in sub-folders, associated with the following topics: boundary conditions (“BC”, Table 5.2); continuity equation (Table 5.3); momentum equation (Table 5.4); transport of solid bodies (Table 5.5); constitutive equation (Table 5.6); boundary treatment scheme “DB-SPH” (Table 5.8); erosion criterion (Table 5.7); geometry/algebra (Table 5.9); initial conditions (“IC”, Table 5.10); main program (“main”), program units for the main code algorithms (both in 2D and 3D), memory management and Leapfrog time integration scheme (Table 5.11); Fortran modules (Table 5.12); neighbouring search, smoothing operators and interface detection (Table 5.13); post-processing (Table 5.14); pre-processing (Table 5.15); boundary treatment scheme “SA-SPH” (Table 5.16); managing Fortran character variables; Runge-Kutta time integration schemes (Table 5.17).

The input files of SPHERA are listed hereafter:

- main input file (user-defined name; the “.inp” format is defined in SPHERA, 2018, [49]);
- file list for the DB-SPH surface meshes (“surface_mesh_list.inp”);
- ensemble of the files of the DB-SPH surface meshes (“.ply” file format).

Folder	Description
(repository folder)	GNU-GPL license file
doc	Documentation file
src	Source code (with makefile)
bin	Executable files compiled with gfortran/ifort for optimized executions
debug	Executable files compiled with gfortran/ifort for debug scalar executions
debug_omp	Executable files compiled with gfortran/ifort for debug parallel executions
input	Input files for tutorials and a commented template for the main input file

Table 5.1. Folders of SPHERA v.9.0.0 repository.

Program unit	Synthetic Description
CancelOutgoneParticles_2/3D	To count and delete the outgoing particles at boundaries
FindFrame/Line	Extreme coordinates of the parallelepiped/rectangle containing the domain
GenerateSourceParticles_2/3D	To generate new source particles at the inlet sections
NormFix, NumberSectionPoints	Minor program units
PreSourceParticles_2/3D	To generate new source particles at the inlet sections (initial time)
VelLaw	To impose an input kinematics to particles

Table 5.2. Program units (“.f90”) for the boundary conditions of the inlet/outlet sections (SPHERA, 2018, [49], folder “BC”).

Program unit	Synthetic Description
CalcPre	To estimate particle pressure
Continuity_Equation	To assess continuity equation RHS, velocity gradients and strain-rate tensor.
inter_SmoothPres	To calculate a corrective term for pressure
PressureSmoothing_2/3D	To execute partial smoothing for pressure

Table 5.3. Program units (“.f90”) for the continuity equation (SPHERA, 2018, [49], folder “BE_mass”).

Program unit	Synthetic Description
Diffumorris	Minor subroutine
inter_EqMoto	To assess the momentum equation RHS and DB-SPH terms
velocity_smoothing/_SA_SPH_2/3D	To assess a corrective term for velocity
viscomon	To assess an artificial viscosity term
viscomorris	To assess the viscous shear stress term in the momentum equation

Table 5.4. Program units (“.f90”) for the momentum equation (SPHERA, 2018, [49], folder “BE_momentum”).

Program unit	Synthetic Description
Body_dynamics_output	To write “.txt” output files for body transport in fluid flows
body_particles_to_continuity	Contributions of the body particles to the continuity equation
body_pressure_mirror	Computation of the body particle pressure
body_pressure_postpro	Post-processing for body particle pressure
body_to_smoothing_pres	Contributions of body particles to pressure partial smoothing
body_to_smoothing_vel	Contributions of body particles to the possible velocity correction term
Gamma_boun	Interpolative function for boundary force particles
Input_Body_Dynamics	Advanced input management for body transport
RHS_body_dynamics	To estimate the RHS of the body dynamics equations

Table 5.5. Program units (“.f90”) for the transport of solid bodies (SPHERA, 2018, [49], folder “Body_Transport”).

Program unit	Synthetic Description
mixture_viscosity	To assess frictional viscosity and mixture viscosity for dense granular flows
Viscapp	Minor subroutine

Table 5.6. Program units (“.f90”) for the constitutive equation (SPHERA, 2018, [49], folder “Constitutive_Equation”).

Program unit	Synthetic Description
compute_k_BetaGamma	Coefficient for Shields parameter in 3D
fixed_bed_slope_limited	Management of mixture particles belonging to the fixed bed
Shields	2-interface 3D erosion criterion

Table 5.7. Program units (“.f90”) for the erosion criterion (SPHERA, 2018, [49], folder “Erosion_Criterion”).

Program unit	Synthetic Description
1 adjacent_faces_isolated_points	Provided 2 adjacent faces, it finds the vertices not in common.
2 BC_wall_elements	To assess wall element density and pressure
3 DBSPH_BC_shear_viscosity_term	Contributions to the numerator of the shear viscosity term
4 DBSPH_find_close_faces	Finding the adjacent surface elements of a given surface element
5 DBSPH_IC_surface_elements	Initialization of wall surface elements
6 DBSPH_inlet_outlet	Imposing boundary conditions at the inlet and outlet sections
7 DBSPH_kinematics	Input kinematics for the DB-SPH elements (interpolation of input data)
8 DBSPH_velocity_gradients_VSL_SNBL	Velocity gradients in the Viscous Sub-Layer
9 Gradients_to_MUSCL	Consistency estimation of velocity and density gradients for MUSCL
10 Gradients_to_MUSCL_boundary	Boundary terms for the MUSCL reconstruction scheme
11 Import_ply_surface_meshes	Managing the surface meshes of SnappyHexMesh
12 semi_particle_volumes	Semi-particle shape coefficients and volumes
13 wall_elements_pp	Smoothing wall element physical quantities for post-processing
14 wavy_inlet	To provide a very slightly wavy flow at the inlet section

Table 5.8. Program units (“.f90”) for the boundary treatment scheme (SPHERA, [49], 2018, folder “DB_SPH”).

Program unit	Synthetic Description
23 area_hexagon/.../triangle	Area of a generic hexagon/.../triangle from of its vertex coordinates
24 dis_point_plane	To assess the distance between a point and a plane
25 distance_point_line_2/3D	To assess the distance between a point and a line in 2/3D
26 IsPointInternal	To check whether a point is internal/external to a given face
27 line_plane_intersection	Intersection point (if unique) between a line and a plane
28 LocalNormalCoordinates	To compute the local normal vectors
29 Matrix_Inversion_2x2/3x3	To assess the inverse of a provided 2x2/3x3 matrix
30 MatrixProduct	To assess the matrix product between two matrices
31 MatrixTransposition	To transpose a matrix
32 point_inout_convex_non_degenerate_polygon	Test to evaluate if a point lies inside or strictly outside a polygon
33 quadratic_equation	To solve a quadratic equation
34 reference_system_change	Transformation of coordinates in a new reference system
35 three_plane_intersection	To assess the intersection between 3 planes
36 Vector_Product	To assess the cross product of two vectors
37 vector_rotation_axis_angle	To provide the rotation angle and axis of a 3D vector rotation
38 vector_rotation_Euler_angles	3D rotation of a given vector, provided the Euler angles.
39 vector_rotation_Rodrigues	3D rotation of a given vector, by means of Rodrigues formula.

Table 5.9. Program units (“.f90”) on geometry/algebra (SPHERA, 2018, [49], folder “Geometry”).

Program unit	Synthetic Description
49 GeneratePart/SetParticles	To set particle initial positions
50 initialization_fixed_granular_particle	To initialize the most of the fixed SPH mixture particles (bed-load transport)
51 IsParticleInternal2/3D	To check whether a particle is internal to the 2/3D domain
52 SetParticleParameters	To set the initial particle quantities
53 SubCalcPreIdro	Hydrostatic pressure profiles (in case they are imposed as initial conditions)

Table 5.10. Program units (“.f90”) for the initial conditions (SPHERA, 2018, [49], folder “IC”).

Program unit	Synthetic Description
Gest_Dealloc	Array deallocations
Gest_Trans	Introductory procedure for the main algorithm
Loop_Irre_2/3D	2/3D main algorithm
sphera	Main program unit

Table 5.11. Program units (“.f90”) for the main algorithms (SPHERA, 2018, [49], folder “Main_algorithm”).

Program unit	Synthetic Description
Dynamic_allocation_module	Module to define the dynamically allocated variables
Hybrid_allocation_module	Module for derived types of both dynamically and statically allocated variables
I_O_diagnostic_module	To provide global interfaces to the subroutine “diagnostic”
I_O_file_module	Module for Input/Output file management
SA_SPH_module	Module for the semi-analytic approach (boundary treatment scheme)
Static_allocation_module	Module to define global and statically allocated variables
Time_module	Module for computational time recording

Table 5.12. Fortran modules (“.f90”; SPHERA, 2018, [49], folder “Modules”).

Program unit	Synthetic Description
CalcVarLength	Neighbouring search (pre-conditioned dynamic vector), SPH operators, interfaces.
CellIndices	To return the indices of the cell (positioning grid) a generic particle belongs to.
Particle/CellNumber	To return the ID of a generic positioning cell
CreaGrid	To create the background positioning grid
InterFix	Minor program unit
OrdGrid1	Ordering the numerical elements on the background positioning grid
w	To assess the kernel functions

Table 5.13. Program units (“.f90”) for the neighbouring search, the smoothing operators and the interface detection (SPHERA, 2018, [49], folder “Neighbouring_Search”).

Program unit	Synthetic Description
calc_pelo	Post-processing to write the free surface height
CalcVarp	To calculate physical quantities at a monitoring point
cat_post_proc	To concatenate the “.txt” output files
CreateSectionPoints/s_ctime	Minor program units
electrical_substations	Substation-flooding damage model
GetVarPart	Getting particle values for monitoring
interface_post_processing	Post-processing the interfaces for bed-load transport phenomena
Memo_Ctl	Post-processing for monitoring lines and points
Memo_Results	To write detailed results for restart
Print_Results	Post-processing for the log file
result_converter	Post-processing for “.vtu” and “.vtk” files for Paraview
start_and_stop	Computational time recording
sub_Q_sections	To write the flow rate at the associated monitoring sections
Update_Zmax_at_grid_vert_columns	Current 2D fields of the water depth and specific flow rate
write_Granular_flows_interfaces	To print the interfaces for bed-load transport phenomena
write_h_max	2D fields of the maximum water depth and specific flow rate

Table 5.14. Program units (“.f90”) for post-processing (SPHERA, 2018, [49], folder “Post_processing”).

Program unit	Synthetic Description
1 defcolpartzero	On the particle colours for visualization purposes
2 Diagnostic	Error message diagnostic
3 Gest_Input	Input check and management
4 Init_Arrays/ReadCheck/ReadInput...	Minor program units
5 ModifyFaces	To generate triangles from quadrilaterals
6 ReadBedLoadTransport	Reading input data for bed-load transport
7 ReadBodyDynamics	Reading input data for solid body transport
8 ReadDBSPH	Reading input data for the DB-SPH boundary treatment scheme
9 ReadInput	Reading input data
10 ReadInputBoundaries	Reading input data for the boundary treatment scheme SA-SPH
11 ReadInputControlLines	Reading monitoring lines
12 ReadInputControlPoints	Reading monitoring points
13 ReadInputControlSections	Reading control sections
14 ReadSectionFlowRate	Input management for the flow rate monitoring sections

Table 5.15. Program units (“.f90”) for pre-processing (SPHERA, 2018, [49], folder “Pre_processing”).

Program unit	Synthetic Description
23 AddBoundaryContribution_to_CE/ME2/3D	To compute boundary terms for the 2/3D continuity/momentum equation
24 BoundaryMassForceMatrix2/3D	Generation of the generalized boundary mass force matrix in 2/3D
25 BoundaryPressureGradientMatrix3D	To generate the pressure gradient matrix
26 BoundaryReflectionMatrix2D	To generate the generalized reflection matrix R
27 BoundaryVolumeIntegrals2D	To compute the boundary volume integrals
28 ComputeBoundaryDataTab	To calculate the array to store close boundaries and integrals
29 ComputeKernelTable/...	Kernel-related parameters and integrals
30 ComputeSurfaceIntegral_WdS2D	Computing kernel surface integrals
31 ComputeVolumeIntegral_WdV2D	Computing kernel volume integrals
32 DefineBoundaryFace/SideGeometry3/2D	Definition of the boundary faces/sides in 3/2D
33 DefineBoundarySideRelativeAngles2D	Detection of the previous adjacent side and associated relative angle
34 DefineLocalSystemVersors	To define the directional cosines of the local reference system
35 FindBoundaryConvexEdges3D	To look for possible edges with an associated convex geometry
36 FindBoundaryIntersection2D	Intersection between a kernel support a boundary side
37 FindCloseBoundaryFaces3D/Sides2D	To finds the "close" boundary faces/sides in 2/3D
38 GridCellBoundaryFacesIntersections3D	To find the boundary faces intercepted by the cells of the positioning grid
39 Interpolate/...	Interpolation of the boundary integrals
40 IWro2dro/J2Wro2/JdWsRn/WIntegr	To compute SA-SPH definite integrals
41 SelectCloseBoundarySides2D	Selecting the neighbouring boundary sides

Table 5.16. Program units (“.f90”) for the boundary treatment scheme SA-SPH (SPHERA, 2018, [49], folder “SA_SPH”).

Program unit	Synthetic Description
53 Euler	Explicit RK1 time integration scheme (Euler scheme)
54 Heun	Heun scheme: explicit RK2 time integration scheme.
55 time_step_duration	Computation of the time step duration according to stability constraints
56 stoptime	Stopping time for computational time recordings
57 time_integration	Explicit Runge-Kutta time integration schemes
58 time_integration_body_dynamics	Leapfrog time integration scheme for solid body transport

Table 5.17. Program units (“.f90”) for time integration (SPHERA, 2018, [49], folder “Time_integration”).

The main output files of SPHERA report the following information:

- application log of SPHERA;
- 3D fields of the main fluid dynamics and SPH variables (“.vtu” and “.pvd” file formats) for Paraview visualization;
- frontier geometry for the boundary treatment SA-SPH (“.vtk” format for Paraview);
- time series of the main fluid dynamics variables (pressure and velocity) along the monitoring lines and points;
- flow rate hydrographs at the flow rate monitoring sections;
- hydrographs of the free surface height at the monitoring lines;
- 2D fields of the maximum values of the specific flow rate and the free surface height;
- time series of the interfaces of the model for dense granular flows;
- output files on the boundary treatment scheme DB-SPH;
- output files on the solid bodies.

6.2. SPHERA v.9.0.0: compilation and execution

SPHERA installation is straightforward, even because a set of executable files are already available as reference. SPHERA source and executable files are distributed on a dedicated Git repository ([49]) on GitHub. SPHERA executable files are released for Linux OS (compilers: both ifort and gfortran, with OpenMP libraries). The Makefile (under the folder “src”) allows compiling SPHERA under different configurations, according to the assignation of the following variables: “EXECUTION” = “bin” (optimized), “debug”; “COMPILATION_FLAGS” = “-O1” (optimized execution), “-g -O0 -fbacktrace -C” (gfortran debug), “-g -O0 -traceback -C -check bounds -check noarg_temp_created -debug all” (ifort debug); “COMPILER” = “gfortran”, “ifort”; “OMP_FLAG” = “-fopenmp” (gfortran omp); “-qopenmp” (ifort omp). Compilation is carried out by two consecutive command lines: “make touch”; “make”.

The only mandatory argument in the command line for executing SPHERA is the name of the main input file (without the format extension “.inp”).

6.3. Main input file of SPHERA v.9.0.0

The folder “input” of the code repository hosts a commented template of the main input file of SPHERA, where all the input parameters are defined, the meaning of their possible values are described and suggested, possible default values are reported. Table 5.18 presents a synthetic description of the contents of the main input file of SPHERA.

Input file section	Synthetic Description
Title	Test case title
Domain	Spatial resolution and choice of the boundary treatment scheme
Vertices	Vertices of the fluid domain boundaries
Lines/Faces	Vertex connections of the boundary lines/faces of the fluid domain in 2/3D
Boundaries	Features of the fluid domain bodies and boundaries (solid boundaries, open/inlet sections): initial conditions, boundary conditions, possible extrusions of water bodies from topography.
DBSPH	Quantities on the DB-SPH boundary treatment scheme, related to: spatial resolution at boundaries, MUSCL reconstruction scheme, geometry of semi-particles, slip conditions, limiters, monitors, number of files for the surface mesh (initial positions of the boundary elements), imposed kinematics (of the boundaries), inlet/outlet sections.
Bed-load transport	Input quantities for the following features: scheme for dense granular flows, erosion criterion, saturation scheme, monitors, liquefaction scheme.
Medium	Input physical quantities on the fluid and solid phase properties and the scheme for dense granular flows: bulk modulus, viscosity, saturation conditions, internal friction angle, limiting viscosity, maximum viscosity, effective porosity, mean diameter of the solid grains.
Body dynamics	Input physical quantities on the scheme for body transport in fluid flows: possible imposed kinematics; number of bodies; spatial resolution within the solid bodies; friction angle; limiters. For each body, the following quantities are requested: number of elements; mass; vectors of the initial position, velocity and angular velocity; tensor of the mass moment of inertia (if this is constant and not computed); initial orientation of the body with respect to the reference system. For each body element, the following quantities are requested: side lengths of the element; vector of the initial position; initial rotation of the element with respect to the reference system; Boolean operator to treat the element when configuring its reference body.
Run parameters	Final time, CFL , C_v and time integration scheme; weight of the partial smoothing; numerical quantities for memory management.
General physical properties	Gravity acceleration vector; reference pressure.
Restart	Frequency for writing the restart files
Output regulation / draw options	Frequency for writing SPHERA output files
Control points	Position of the monitoring points
Control lines	Position and discretization of the monitoring lines
Section flow rate	Geometry of the monitoring sections for the flow rate
Substations	Geometries of the electrical substations for the substation-flooding damage scheme and substation type (high-voltage transmission substation, medium-voltage distribution substation, low-voltage distribution substation). Each substation is described by a polygon.

Table 5.18. Sections and relevant quantities of the main input file of SPHERA v.9.0.0 ([49]).

7. MODELLING CHAIN OF SPHERA

1 An overview of the numerical modelling chain of SPHERA (Figure 5.1) is herein discussed.

2
3
4 The dataset SRTM3 (USGS, 2014, [51]) provides a repository of DEM (“Digital Elevation
5
6
7
8
9
10
11
12
13
14
15
16
17
18
19
20
21
22
23
24
25
26
27
28
29
30
31
32
33
34
35
36
37
38
39
40
41
42
43
44
45
46
47
48
49
50
51
52
53
54
55
56
57
58
59
60
61
62
63
64
65
Models”) with an almost global cover and spatial resolution of 1” (in terms of geographical coordinates) or ca.31m (maximum/coarser spatial resolution in terms of cartographic coordinates). With respect to the former free DEM datasets (finest spatial resolution of 3”), SRTM3 has permitted a relevant improvement in using Open-Access DEM. The SRTM3 products are available in the format “.tif”. Considering its global coverage, SRTM3 provides a root-mean-square error on heights of ca.6m, even though the error kurtosis is very high (Rexer & Hirt, 2014, [45]). However, these estimations refer to almost the whole terrestrial surface, included the high-latitude regions where errors are definitely higher.

26
27
28
29
30
31
32
33
34
35
36
37
38
39
40
41
42
43
44
45
46
47
48
49
50
51
52
53
54
55
56
57
58
59
60
61
62
63
64
65
The software tool GDAL (OSGEO, [22]), the main QGIS library, can be used as an independent code. In the frame of the present modelling chain, GDAL allows to convert the DEM file format “.tif” of SRTM3 in the alternative format “.dem”.

34
35
36
37
38
39
40
41
42
43
44
45
46
47
48
49
50
51
52
53
54
55
56
57
58
59
60
61
62
63
64
65
DEM2xyz (RSE SpA, [49]) reads the DEM file (“.dem” format), converts the geographic coordinates in Cartesian coordinates over a regular grid and writes the resulting DEM on an output file (“.xyz” format), possibly coarsening the spatial resolution.

41
42
43
44
45
46
47
48
49
50
51
52
53
54
55
56
57
58
59
60
61
62
63
64
65
Paraview (Kitware, [42]) reads the “.xyz” output file of DEM2xyz and elaborates a 2D Delaunay grid starting from the DEM vertices. Paraview also allows to cut the numerical domain (the cuts have to be far enough from the water bodies not to disable the procedures to extrude the water bodies from the DEM), circumscribes the water bodies, draws the possible filing/digging regions, detects the dam toe and the most upstream point over the coastline of the water bodies.

53
54
55
56
57
58
59
60
61
62
63
64
65
The above information, derived from Paraview, is transferred over the main input file of DEM2xyz, which is executed again to modify the already computed DEM, by reconstructing the bathymetry below the water bodies and the possible assignation of the digging/filling regions (uniform height within the same region), after a verification/modification on the normal vectors to the surface

1 elements of the DEM. At this point, Paraview is used again to draw those geometrical figures which
2 are necessary to initialize some variables in the main input file of SPHERA, in order to detect water
3 bodies, earth-filled dams and monitoring elements.
4

5
6
7 The numerical tool ply2SPHERA_perimeter (RSE SpA, [49]) converts the DEM “.ply” file in two
8 distinct output files. They have the same format as the sections “VERTICES” and “FACES” of the
9 main input file of SPHERA. It is the vertices and faces of the portion of the DEM within the
10 numerical domain of SPHERA.
11
12
13
14
15

16
17 In case the boundary treatment method of Sec.4 is used, SnappyHexMesh (OpenFOAM, OpenCFD
18 Ltd, [39]) is used as a surface grid generator for the initial positioning grid of the DB-SPH
19 elements.
20
21
22

23
24 Once the sections “VERTICES” and “FACES” are obtained from ply2SPHERA_perimeter and the
25 input file for the positioning surface grid is produced by SnappyHexMesh, one completes the
26 remaining sections of the main input file of SPHERA. This 3D CFD-SPH code is then executed.
27
28
29
30

31 The output files of SPHERA which contain the profiles (1D) of the fluid dynamics variables are
32 visualized by means of Gnuplot (Williams & Kelley, [23]), which returns the output files in the
33 “.eps” format. These files are read by GSView (Ghostgum Software Pty Ltd, [25]) and converted in
34 the “.png” format. The profiles simulated are compared with the analogous experimental (or
35 numerical) profiles available from experimental images or the scientific literature (indexed journals;
36 Open-Data archives). In this instance, it is normally admitted the digitization of experimental and
37 numerical profiles from published sources by means of Engage Digitizer (Mitchell et al., [19]), with
38 proper citation of the source, in order to validate the code.
39
40
41
42
43
44
45
46
47
48
49

50
51 The output files of SPHERA which contains the synthetic fluid dynamics fields need a following
52 elaboration by means of Grid Interpolator (RSE SpA, [49]).
53
54
55
56
57
58
59
60
61
62
63
64
65

1
2
3
4
5
6
7
8
9
10
11
12
13
14
15
16
17
18
19
20
21
22
23
24
25
26
27
28
29
30
31
32
33
34
35
36
37
38
39
40
41
42
43
44
45
46
47
48
49
50
51
52
53
54
55
56
57
58
59
60
61
62
63
64
65

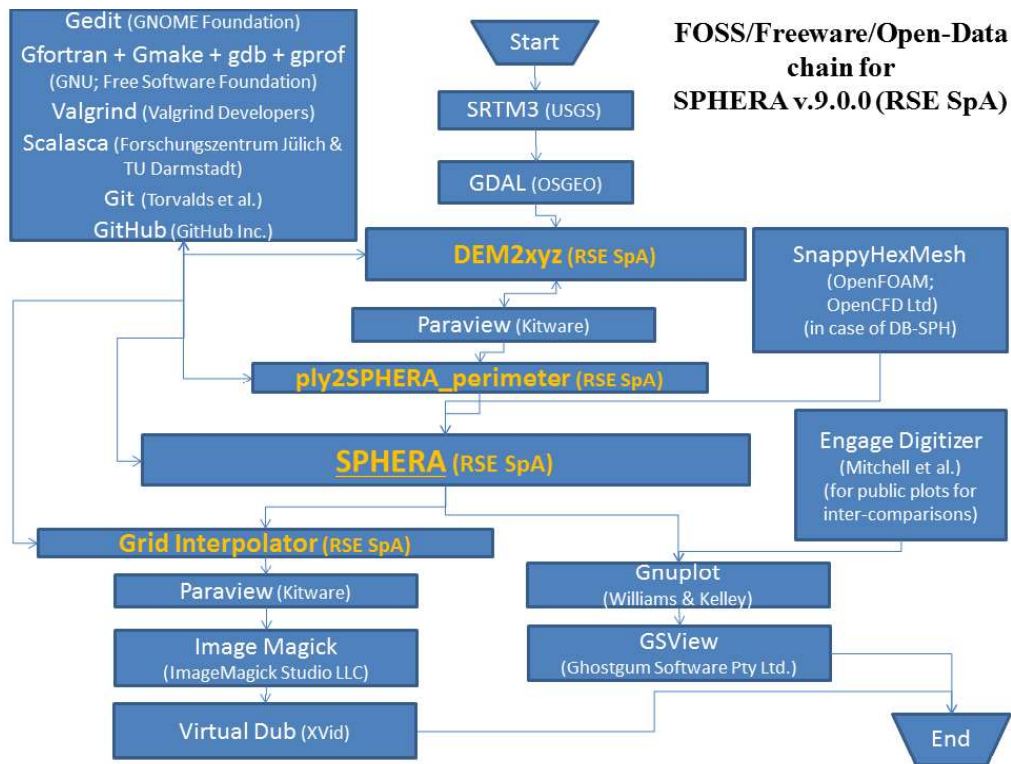


Figure 5.1. Free tools of the numerical chain of SPHERA v.9.0.0.

Paraview shows the 2D and 3D fluid dynamics fields produced by SPHERA and returns the associated image files. These are concatenated in “.gif” animations by means of Image Magick (ImageMagick Studio LLC, [28]). The compression of these animations, necessary in case the concatenation involves many files, is carried out by means of Virtual Dub ([60]), which returns an “.avi” video output file.

The numerical modelling chain is based on free tools: FOSS, freeware or OpenData. All the items of the chain are FOSS, but the “Freeware” tools (GitHub for public repositories and GSView; they are simply free) and SRTM3, which is “Open-Data” (dataset available upon public and free access). It is possible to support or replace the auxiliary tools of the modelling chain with more effective software, if available (e.g., commercial compilers; DEM files with finer spatial resolutions than SRTM3). The replacement of a free tool with a proprietary tool (with charge) is normally a reversible procedure which does not alter the functioning of the modelling chain.

8. TUTORIALS, VALIDATIONS AND APPLICATIONS

SPHERA v.9.0.0 has been validated and applied on more than forty test cases, included the 34 tutorials of the code repository, whose input files are updated with the last code release. Each tutorial has up to seven configuration variants. Some of the test cases of SPHERA are described in the following sub-sections and refer to either papers on International Journals or studies in progress. The aim of this section is just to recall the code tutorials, and other validations and applications. However, the images shown here are unpublished and those studies in progress are only recalled in terms of previews. The references for details and validations on the single test cases are available in each of the following sub-sections.

8.1. Floods

The most applications of SPHERA refer to floods (Figure 5.2). SPHERA has simulated floods on real and complex topographies (domain spatial coverage up to some hundreds of squared kilometres) with transport of solid bodies, bed-load transport, flood-control works and the assessment of the flood-induced damage related to the functioning of the electrical substations.

8.1.1. 2D impact of a water liquid jet on a flat plate

A 2D water liquid jet impacts a solid flat plate. An exact analytical solution is available for validation purposes. This very simplified configuration is introductory to any fluid-boundary and fluid-body interaction occurring during floods, landslides and wave motion (Sec.8.1.19), sediment removal from water bodies (Sec.8.3) and sloshing tanks (sec.8.4). The seven variants of this tutorial (SPHERA v.9.0.0, 2018, [49], folder “jet_plate”) refer to Amicarelli et al. (2013, [5]) and Amicarelli et al. (2015, [6]).

8.1.2. Impact of a 2D dam-break frontal wave on a solid vertical wall

Two advanced boundary treatment techniques of SPHERA are in the process of being further validated on 2D dam break flows in laboratory experiments by Lobosvsky et al. [45], numerically reconstructing the time trend of the primary wave pressures acting on the solid vertical wall downstream and the primary and secondary wave height at specific positions along the channel

1
2
3
4
5
6
7
8
9
10
11
12
13
14
15
16
17
18
19
20
21
22
23
24
25
26
27
28
29
30
31
32
33
34
35
36
37
38
39
40
41
42
43
44
45
46
47
48
49
50
51
52
53
54
55
56
57
58
59
60
61
62
63
64
65

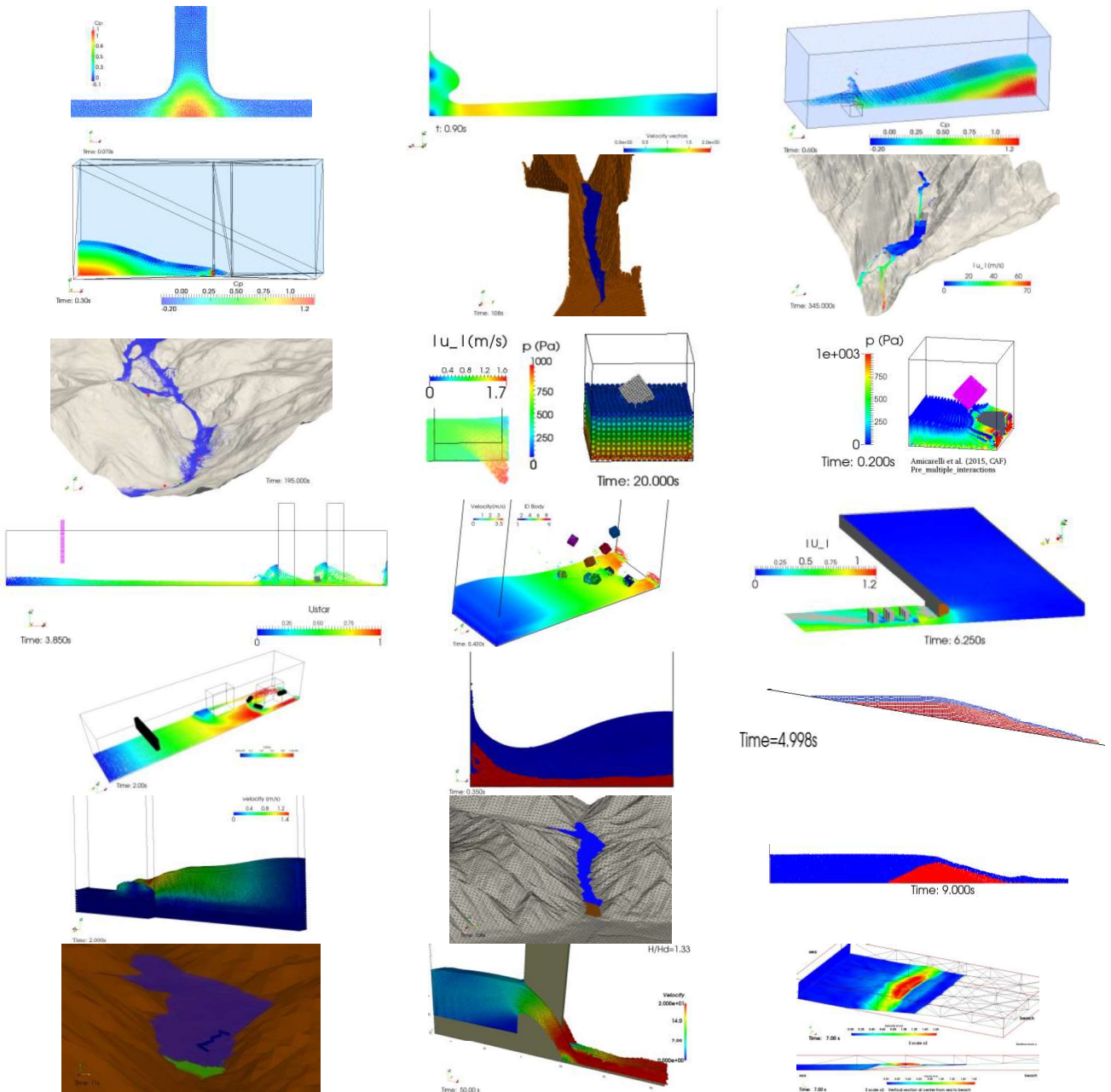


Figure 5.2. Tutorials, validations and applications: floods. The test cases are shown from the left to the right panel, and from the top to the bottom row, following the section numbering. First row: 2D impact of a water liquid jet on a flat plate; impact of a 2D dam-break frontal wave on a solid vertical wall; impact of a dam-break flood front over a squat obstacle. Second row: impact of a dam-break flood front over a tall obstacle; dam break on complex topography; dam-break scenarios for the concrete dam of Alpe Gera. Third row: propagation of the Alpe Gera dam-break flood on the residential areas and the electrical substations of the municipality of Lanzada; sub-critical flow passing by a rectangular side weir; stability of a floating cube; impact of a dam-break flood front over two solid bodies. Fourth row: transport of a floating body during a dam-break flood with fixed obstacles; impact of a dam-break flood front over nine solid bodies; urban dam-break flood scenarios. Fifth row: urban flood with the transport of large floating bodies; 2D erosional dam breaks; erosional dam break on a 2D slope. Sixth row: 3D laboratory erosional dam-break flood; erosional dam break on complex topography; dike overtopping. Seventh row: dam-breach flood with transport of tree trunks; spillway with pier (USACE benchmark); tsunami (ISEC benchmark n.1).

(Mirauda D., R. Albano, A. Amicarelli, in progress). The first employed boundary treatment technique (Sec.2.1) is based on the computation of volume integrals within the truncated portions of

1 the kernel supports at boundaries; the second one (Sec.2.3) stems from the extension of the ghost-
2 particle boundary method for mobile boundaries adapted to free-slip conditions.
3

4 **8.1.1. Impact of a dam-break flood front over a squat obstacle**

5 This tutorial (SPHERA v.9.0.0, 2018, [49], folder “db_squat_obstacle”; Amicarelli et al., 2013, [5])
6
7 permits to validate the code on a controlled laboratory test representing a 3D dam-break flood
8
9 whose front impacts a squat obstacle.
10
11
12

13 **8.1.2. Impact of a dam-break flood front over a tall obstacle**

14 This tutorial (SPHERA v.9.0.0, 2018, [49], folder db_tall_obstacle; Amicarelli et al., 2013, [5])
15
16 permits to validate the code on a further laboratory test representing a 3D dam-break flood whose
17
18 front impacts a tall obstacle.
19
20
21
22

23 **8.1.3. Dam break on complex topography**

24 This tutorial (SPHERA v.9.0.0, 2018, [49], folder “db_ICOLD”) provides a demonstrative study (in
25
26 progress beyond a minor publication) of an instantaneous and complete break of a concrete dam
27
28 whose flood propagates on a complex and full-scale topography.
29
30
31
32

33 **8.1.4. Dam-break scenarios for the concrete dam of Alpe Gera**

34 This tutorial (SPHERA v.9.0.0, 2018, [49], folder “db_Alpe_Gera”) represents the full-scale
35
36 representation of three dam-break scenarios involving the highest Italian working concrete dam
37
38 (Alpe Gera) and the downstream concrete dam of Campo Moro. Flood propagates on real
39
40 topography and a flood-control work is simulated. This study is in progress beyond a minor
41
42 publication.
43
44
45
46
47

48 **8.1.5. Propagation of the Alpe Gera dam-break flood on the residential areas and** 49 **the electrical substations of the municipality of Lanzada**

50 This tutorial (SPHERA v.9.0.0, 2018, [49], folder “db_Alpe_Gera_Lanzada_substations”) simulates
51
52 the follow-up of one of the scenarios of Sec.8.1.4 over a down-stream domain involving four
53
54 residential areas and two electrical substations of the municipality of Lanzada (Sondrio, Italy),
55
56 whose flooding-related damage is assessed in terms of black-out event quantities and costs to
57
58
59
60
61
62

1 restore the electrical components of the substations. This study is in progress beyond a minor
2 publication.
3

4 **8.1.6. Sub-critical flow passing by a rectangular side weir**

5
6
7 This tutorial (SPHERA v.9.0.0, 2018, [49], folder “rectangular_side_weir_Fr_0_491”) reproduces a
8
9 laboratory experiment on the stationary regime of a sub-critical free-surface flow ($Fr=0.491$)
10
11 passing by a rectangular side weir. This study is in progress beyond a minor publication.
12
13

14 **8.1.7. Stability of a floating cube**

15
16
17 This simple and demonstrative tutorial (SPHERA v.9.0.0, 2018, [49], folder
18
19 “floating_cube_stability”) represents a solid cube leaned on still water at a rough spatial resolution.
20
21
22 This test is introductory to more complex applications dealing with the transport of solid bodies
23
24 within fluid flows. This study is in progress beyond a minor publication.
25
26

27 **8.1.8. Impact of a dam-break flood front over two solid bodies**

28
29 This demonstrative tutorial (SPHERA v.9.0.0, 2018, [49], folder “db_2bodies”; Amicareli et al.,
30
31 2015, [6]) represents a simplified dam break-flood front which impacts two solid bodies. Fluid-
32
33 body, body-body and body-boundary interactions are solicited at a very coarse spatial resolution to
34
35 demonstrate the absence of penetrations between the masses of the several media involved.
36
37
38

39 **8.1.9. Transport of a floating body during a dam-break flood with fixed** 40 41 **obstacles**

42
43
44 This tutorial (SPHERA v.9.0.0, folder “db_body_exp_UniBas”; Amicareli et al., 2015, [6])
45
46 simulates the transport of a floating solid body during a dam-break flood. The body interacts with
47
48 the flood, two fixed obstacles and the solid boundaries of the domain. Validation is documented by
49
50 comparing the numerical results with the available measures.
51
52
53

54 **8.1.10. Impact of a dam-break flood front over nine solid bodies**

55
56 This tutorial (SPHERA v.9.0.0, 2018, [49], folder “db_multi_body”; Amicarelli et al., 2015, [6])
57
58 simulates the impact of a simple dam-break flood over nine solid bodies (with different weights),
59
60
61
62
63
64
65

1 juxtaposed at the beginning of the simulation to form a vertical plate. Multiple body-body
2 interactions are simultaneous to fluid-boundary and body-boundary interactions.
3

4 **8.1.11. Urban dam-break flood scenarios**

5 This tutorial (SPHERA v.9.0.0, 2018, [49], folder “SPH_udb_exp_Kim2015HYDROL”) represents
6
7 the SPH simulation of two scenarios of a laboratory urban dam-break flood for validation purposes.
8
9 This study is in progress beyond a minor publication.
10
11
12

13 **8.1.12. Urban flood with the transport of large floating bodies**

14 Albano et al. (2016, [46]) simulated a 3D complex configuration involving the multiple transport of
15
16 rigid bodies in free surface flows. SPHERA was validated in a sequence of laboratory test cases
17
18 carried out in Albano et al. (2016, [46]) on a rectangular tilting flume, which schematized the
19
20 failure of a small dam affecting an urban floodplain near buildings and vehicles. The model showed
21
22 a good reliability, in terms of water depth time evolution and time history of the body trajectories,
23
24 demonstrating that it has reached a level of maturity that allows for quantitative comparison with
25
26 complex experimental measurements; in this light, the model has demonstrated as a cost-efficient
27
28 tool for urban flood analysis providing additional information that cannot be easily obtained from
29
30 direct experimental observation such as water flow pressure and velocity.
31
32
33
34
35
36
37
38

39 **8.1.13. 2D erosional dam breaks**

40 An erosional dam break is represented by a dam-break flood propagating over a mobile bed.
41
42 SPHERA demonstrative tutorial “edb_2D_demo” (SPHERA v.9.0.0) is represented in Figure 5.2
43
44 (13th panel). Four other tutorials deal with validation and model inter-comparisons on erosional dam
45
46 breaks (SPHERA v.9.0.0, 2018, [49], folders “edb_KarlSand”, “edb_2D_FraCap02”,
47
48 “edb_2D_Spi05”, “edb_2D_FraCap02_Taipei”; Amicarelli et al. 2017, [7]). These erosional dam
49
50 breaks are also introductory to the more complex configurations of the following sub-sections.
51
52
53
54
55
56
57
58
59
60
61
62
63
64
65

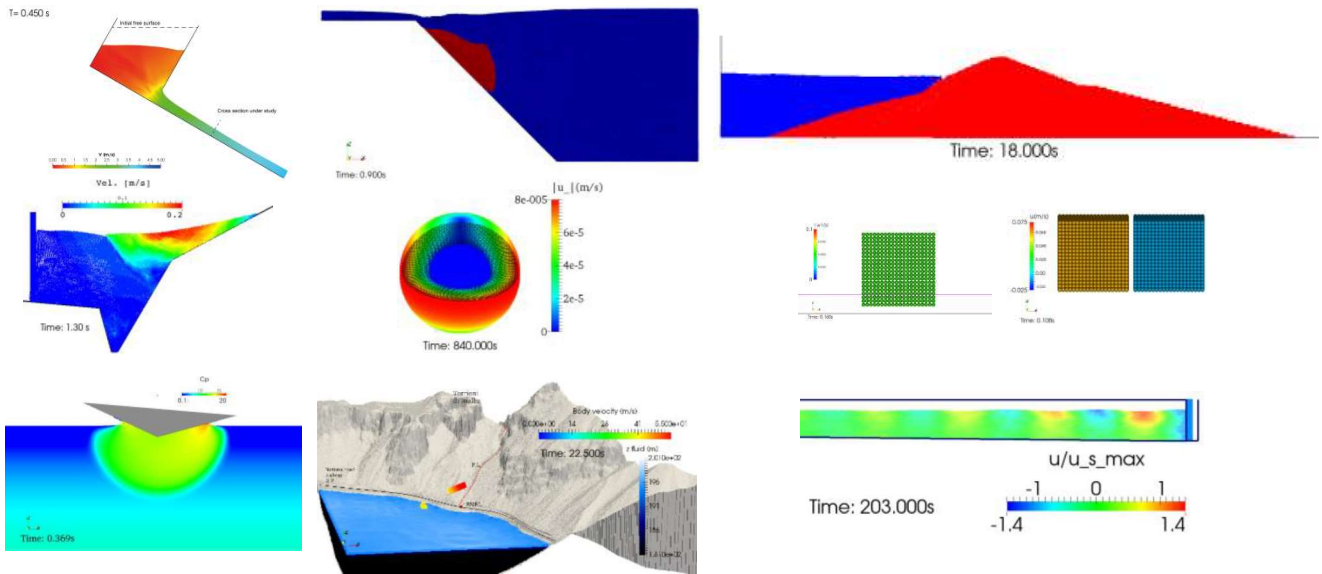


Figure 5.3. Tutorials, validations and applications: landslides and wave motion. The test cases are shown from the left to the right panel, and from the top to the bottom row, following the section numbering. First row: laboratory dry granular flows; 2D submerged landslide; liquefaction of San Fernando Lower dam. Second row: 2D Vajont experiment (landslide and tsunami); spherical Couette flows; body-boundary and body-body impingements. Third row: 2D free falls of solid wedges on still water; Torrioni di Rialba rock-toppling runout and landslide-water impact simulation; swell sea wave.

8.1.14. Erosional dam break on a 2D slope

A 2D collapse of granular-liquid mixture over rigid inclined flatbed is represented (Ziane, Khellaf, Amicarelli; in progress). The validation is documented by comparing the numerical front position of the mixture with the available measures (Berzi et al., 2012, [9]).

8.1.15. 3D laboratory erosional dam-break flood

This erosional dam-break flood represents a tutorial (SPHERA v.9.0.0, 2018, [49], folder “edb_Pon10”) which provides a code validation described in Amicarelli et al. (2017, [7]).

8.1.16. Erosional dam break on complex topography

This erosional dam-break flood represents a demonstrative tutorial (SPHERA v.9.0.0, 2018, [49], folder “edb_ICOLD”; Amicarelli et al., 2017, [7]) on complex topography.

8.1.17. Dike overtopping

This tutorial (SPHERA v.9.0.0, 2018, [49], folder “dike_breach_2D_expSchHag12JHR_ID22”) represents the SPH simulation of a laboratory dike overtopping to validate the code on a riverine flood. This study is in progress beyond a minor publication.

8.1.18. Dam-breach flood with transport of tree trunks

This tutorial (SPHERA v.9.0.0, 2018, [49], folder “dam_breach_ICOLD_trunks”) represents a flood, which is induced by a dam breach (i.e. break of an earth-filled dam by the propagation of a breach channel), propagates on complex topography and transports five solid trunks. This study (in progress beyond a minor publication) simultaneously involves the transport of granular material and solid bodies during a flood event.

8.1.19. Spillway with pier (USACE benchmark)

This tutorial (SPHERA v.9.0.0, 2018, [49], folder “spillway_withpiers”) represents the SPH simulation of a spillway with pier under rising flood levels. The laboratory test of uncontrolled overflow spillway crest (with pier) are reproduced for validation purposes.

8.1.20. Tsunami (ISEC benchmark n.1)

This tutorial (SPHERA v.9.0.0, 2018, [49], folder “tsunami_benchmark1_ISEC”) represents the SPH simulation of transient wave propagation of a tsunami wave attack toward beach. The results are compared with the experiment for validation purposes.

8.2. Landslides and wave motion

SPHERA has represented several fast landslides in rocks or granular material (Figure 5.3), in terms of laboratory and full-scale configurations on real topographies, their possible interaction with water bodies and the associated wave motion.

8.2.1. Laboratory dry granular flows

Following the work presented in [56]-[46], G. Viccione, B. Tagliaferro and L. Sarno (in progress) explore the capability of SPHERA to numerically reproduce dry granular flows which kinematics is depending both on the collisional and frictional momentum exchanges ([51]). Results show the development of a hypercritical fluid flow (being the Froude number $F_r \gg 1$) at the cross section under investigation.

8.2.2. 2D submerged landslide

This tutorial (SPHERA v.9.0.0, 2018, [49], folder “submerged_landslide”) represents a laboratory submerged landslide triggering a tsunami wave. This study (in progress beyond a minor publication) aims to validate the code on a fast landslide and its interaction with a water reservoir.

8.2.3. Liquefaction of San Fernando Lower dam

This tutorial (SPHERA v.9.0.0, 2018, [49], folder “San_Fernando_Lower_..._dam_liquefaction”) represents the real full-scale liquefaction of San Fernando Lower dam (USA, 1971) triggered by an earthquake of $M=6.6$. This study (in progress beyond a minor publication) aims to validate the scheme for liquefaction and applying the code on a complex landslide which interacts with a hydroelectric reservoir.

8.2.4. 2D Vajont experiment - Padua Hydraulic Laboratory (1968)

This tutorial (SPHERA v.9.0.0, 2018, [35], folder “2D_Vajont_experiment”; Manenti et al., 2018, [25]) represents a characteristic cross-section of the Vajont artificial basin reproduced in the scale model of Padua (1968) for evaluating the effect of landslide falling velocity on the maximum wave run-up. This test allows evaluating the landslide-water coupled dynamics (with both stored and pore water) and code validation can be attained through the experimental measures.

8.2.5. Spherical Couette flows

This tutorial (SPHERA v.9.0.0, 2018, [49], folder “spherical_Couette_flows”) represents three configurations of 3D spherical Couette flows (i.e. a fluid shell moving between two rotating solid spheres). Thanks to analytical solutions available, this test case (in progress beyond a minor publication) aims to validate the code under laminar regimes (commonly recorded in dense granular flows), the treatment of mobile boundaries and the propagation of the shear stress waves induced. These features are also introductory to represent earthquake-induced landslides.

8.2.6. Body-boundary and body-body impingements

These tutorials (SPHERA v.9.0.0, 2018, [49], folders “body_boundary_impacts” and “body_body_impacts”; Amicarelli et al., 2015, [6]) represents five configurations of body-boundary

1 and body-body impingements, provides a code validation by comparison with analytical solutions
2 and introduces to the applications on rock landslides with topography. These tutorial are also
3 relevant for the transport of solid bodies during floods.
4
5

6 **8.2.7. 2D free falls of solid wedges on still water**

7
8
9 This tutorial (SPHERA v.9.0.0, 2018, [49], folder “wedge_falls_on_still_water”; Amicarelli et al.,
10 2015, [6]) represents four 2D configurations of free falls of solid wedges on the free surface of a
11 still water reservoir. This test case represents the first stage of the interaction between a falling rock
12 and a water body and provides several code validations by comparisons with the available
13 measures. This tutorial is also relevant for the transport of solid bodies during floods.
14
15
16
17
18
19
20

21 **8.2.8. Torrioni di Rialba rock-toppling runout and landslide-water impact** 22 **simulation**

23
24
25
26 This test case (Longoni et al., in progress) deals with the 3D modelling of a rock-topple landslide.
27 The proposed case study is focused on Torrioni di Rialba: 135-metre high rock cliff that are facing
28 on Como Lake. They are subjected to instability problems due to their geological setting as
29 described in Brambilla et al. ([10]). SPHERA simulates different landslide collapse scenarios and
30 runouts. Simulation starts from the rock impact with the terrain, goes on with its sliding along the
31 300m slope below it, continues with its impact with Como Lake and it ends with the surface wave
32 propagation. This test case is a first example of the use of a numerical method to represent a
33 toppling event in 3D, including the run-out phase and the interaction with a water body.
34
35
36
37
38
39
40
41
42
43
44
45

46 **8.2.9. Swell sea wave**

47
48 This tutorial (SPHERA v.9.0.0, 2018, [49], folder “wave_motion_for_WaveSAX”) represents an
49 introductory and demonstrative test case on the generation, propagation and dissipation of a swell
50 sea wave over a 3D inclined and simplified bathymetry. This study is in progress beyond a minor
51 publication.
52
53
54
55
56
57
58
59
60
61
62
63
64
65

8.3. Sediment removal from water bodies

1
2 A 2D laboratory test reproduces a small-scale idealized flushing manoeuvre induced by the opening
3
4 of the dam bottom outlet in a long, narrow artificial basin. The coupled water-sediment dynamics
5
6 can be suitably simulated (Manenti et al., 2012, [26]), as shown by the comparison between
7
8 experimental and calculated final sediment profile (Figure 5.4, left panel).
9

10
11 Further, SPHERA has simulated two demonstrative processes on sediment removal from a water
12
13 reservoir by means of the opening of a discharge channel (i.e. flushing; Figure 5.4, left panel). The
14
15 associated tutorials (SPHERA v.9.0.0, 2018, [49], folders “flushing_2D” and “flushing_3D”)
16
17 analyse 2D and
18

19
20
21 3D demonstrative and simplified configurations to assess different erosion criteria and further
22
23 validate the scheme for dense granular flows. This study is in progress beyond a minor publication.
24
25

8.4. Sloshing tanks

26
27
28 SPHERA has been validated on two 2D sloshing tanks (Figure 5.4, centre panel). These test cases
29
30 are introductory to the application fields of fuel sloshing tanks and seismic dampers. These tutorials
31
32 (SPHERA v.9.0.0, “sloshing_tank_TbyTn_1_07” and “sloshing_tank_TbyTn_0_78”; Amicarelli et
33
34 al., 2013, [5]) permitted to validate the code on the measures of 2D laboratory sloshing tanks with
35
36 resonance or beats (the period of the force imposed to the tank is 1.07 or 0.78 times the sloshing
37
38 natural period of the tanks, which are partially filled with water).
39
40
41
42

8.5. Viscous flow modelling for hydrodynamic lubrication problems

43
44
45 A further development of SPHERA to treat hydrodynamic lubrication between bodies, considering
46
47 a viscous fluid trapped between a rigid surface and a slider, is under investigation (Amicarelli A. &
48
49 M. Paggi, study in progress). Historically, this topic is of great interest in tribology, where
50
51 lubrication is used to reduce frictional resistances to relative motion of machine elements. SPHERA
52
53 predictions have been validated in relation to the simulation of thin-film viscous fluid flow in slider
54
55 bearings with parallel or linearly diverging profiles, where closed-form solutions are available, see
56
57
58
59
60
61
62
63
64
65

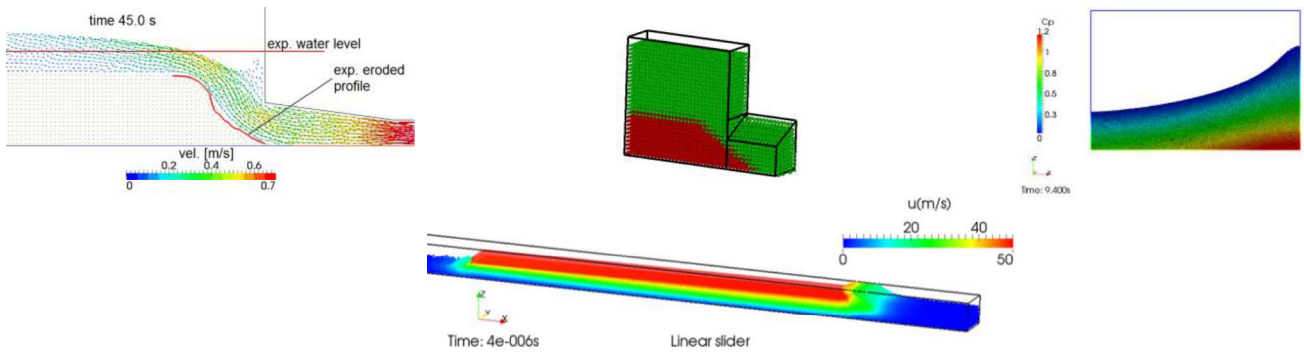


Figure 5.4. Tutorials, validations and applications. First row: 2D sediment flushing (left panel); demonstrative test cases on sediment removal from water bodies (centre panel); sloshing tanks (right panel). Second row: linear slider bearing.

Almqvist et al. (2014, [44]) for an overview of lubrication problems and Paggi & He (2015, [41]) and Paggi & Ciavarella (2010, [40]) for the analysis of the relative motion between two rough surfaces. In this regard, SPHERA is opening new perspectives for modelling and simulation of complex hydrodynamic lubrication problems involving complex textured or rough surfaces, possibly bio-inspired by nature, for which no closed-form solutions are available to characterize their performance.

9. CONCLUSIONS

SPHERA v.9.0.0 (RSE SpA) is a CFD-SPH research code featured by several numerical schemes dealing with: transport of solid bodies in fluid flows; treatment of fixed and mobile solid boundaries; dense granular flows and erosion criteria. SPHERA v.9.0.0 is suitable for the following application fields: floods with transport of solid bodies and bed-load transport; fast landslides and their interactions with water reservoirs; sediment removal from water bodies; fuel sloshing tanks; viscous flow modelling for hydrodynamic lubrication problems. SPHERA is developed and distributed on a GitHub public repository (SPHERA, 2018, [49]) with more than thirty tutorials, thus allowing the code availability and possible modification, and the repeatability of the published test cases. The whole numerical chain of SPHERA is free.

Acknowledgements.

SPHERA has been financed by the Research Fund for the Italian Electrical System (for “Ricerca di Sistema -RdS-”), at different stages:

- ✓ under the second period of RdS (2003-2005), where CESI SpA was the only beneficiary of the Research Fund for the Italian Electrical System;
- ✓ under the Contract Agreement between CESI Ricerca SpA and the Italian Ministry of Economic Development for the of RdS period 2006-2008, in compliance with the Decree of 8 March 2006;
- ✓ under the Contract Agreement between ERSE and the Ministry of Economic Development-General Directorate for Energy and Mining Resources (for the of RdS period 2009-2011) stipulated on 29 July 2009 in compliance with the Decree of 19 March 2009;
- ✓ under the Contract Agreement between RSE SpA and the Italian Ministry of Economic Development for the of RdS period 2012-2014, in compliance with the Decree of November 9, 2012;
- ✓ under the Contract Agreement between RSE SpA and the Italian Ministry of Economic Development for the RdS period 2015-2017, in compliance with the Decree of 21 April 2016. Reference project: ‘A.5 - Sicurezza e vulnerabilità del sistema elettrico’, Frigerio A. et al., 2015-2018.

“We acknowledge the CINECA award under the ISCRA initiative, for the availability of High Performance Computing resources and support.” In fact, SPHERA validation has also been financed by means of the following instrumental funding HPC projects: HSPHCS9, HSPHERA9, HPCEFM18, FLR-RMPV, TNMRA01, HPCEFM7b, HPCEFM17, NMTFEPRA, HPCEFM16, HPCEFM15, HSPHMI14.

The release of the FOSS versions of SPHERA has been supported and promoted by the RSE Department Director Michele de Nigris (during the period 2015-2018) and the RSE Research Team Managers Guido Pirovano (during the period 2016-2018) and Massimo Meghella (during the period 2015-2016).

References.

- 1
2
3
4
5
6
7
8
9
10
11
12
13
14
15
16
17
18
19
20
21
22
23
24
25
26
27
28
29
30
31
32
33
34
35
36
37
38
39
40
41
42
43
44
45
46
47
48
49
50
51
52
53
54
55
56
57
58
59
60
61
62
63
64
65
1. Abdelrazek A.M., I. Kimura, Y. Shimizu; 2016; Simulation of three-dimensional rapid free-surface granular flow past different types of obstructions using the SPH method; *Journal of Glaciology*, 62(232):335-347.
2. Adami S., X.Y. Hu, N.A. Adams; 2012; A generalized wall boundary condition for smoothed particle hydrodynamics; *Journal of Computational Physics*, 231:7057–7075.
3. Albano R., A. Sole, D. Mirauda, J. Adamowski; 2016; Modeling Large Floating Bodies in Urban Floods via a Smoothed Particle Hydrodynamics Model; *Journal of Hydrology*, 541(A):344-358.
4. Almqvist A., Fabricius J, Larsson R, Wall P; 2014; A new approach for studying cavitation in lubrication; *Journal of Tribology*, 136(1):011706
5. Amicarelli A., G. Agate, R. Guandalini; 2013; A 3D Fully Lagrangian Smoothed Particle Hydrodynamics model with both volume and surface discrete elements; *International Journal for Numerical Methods in Engineering*, 95: 419–450, DOI: 10.1002/nme.4514.
6. Amicarelli A., R. Albano, D. Mirauda, G. Agate, A. Sole, R. Guandalini; 2015; A Smoothed Particle Hydrodynamics model for 3D solid body transport in free surface flows; *Computers & Fluids*, 116:205–228. DOI 10.1016/j.compfluid.2015.04.018
7. Amicarelli A., B. Kocak, S. Sibilla, J. Grabe; 2017; A 3D Smoothed Particle Hydrodynamics model for erosional dam-break floods; *International Journal of Computational Fluid Dynamics*, 31(10):413-434; DOI 10.1080/10618562.2017.1422731 ; JCR Impact Factor: 0.983.
8. Armstrong L.M., S. Gu, K.H. Luo; 2010; Study of wall-to-bed heat transfer in a bubbling fluidised bed using the kinetic theory of granular flow; *International Journal of Heat and Mass Transfer*, 53(21-22):4949-4959.
9. Berzi D., F.C. Bossi, E. Larcari; 2012; Collapse of granular-liquid mixtures over rigid, inclined beds; *PHYSICAL REVIEW E* 85, 051308:1-5.
10. Brambilla D., V.I. Ivanov, L. Longoni, D. Arosio, M. Papini; 2017; Geological Assessment and Physical Model of Complex Landslides: Integration of Different Techniques. In *Workshop on World Landslide Forum*:431-437; Springer, Cham.

11. Bui Ha H., R. Fukagawa, K. Sako, S. Ohno; 2008; Lagrangian meshfree particles method (SPH) for large deformation and failure flows of geomaterial using elastic–plastic soil constitutive model; *Int. J. Numer. Anal. Meth. Geomech.*, 32:1537–1570.
12. Colagrossi A., M. Landrini; 2003; Numerical simulation of interfacial flows by smoothed particle hydrodynamics, *Journal of Computational Physics*, 191-2, 448-475.
13. Colagrossi A., A. Souto-Iglesias, M. Antuono, S. Marrone; 2013; Smoothed-particle-hydrodynamics modeling of dissipation mechanisms in gravity waves; *Physical Review E - Statistical, Nonlinear, and Soft Matter Physics*, 87(2), art. no. 023302.
14. Crespo A.J.C., C. Altomare, J.M. Domínguez, J. González-Cao, M. Gómez-Gesteira; 2017; Towards simulating floating offshore oscillating water column converters with Smoothed Particle Hydrodynamics; *Coastal Engineering* (126):11-26.
15. Crespo A.J.C., M. Gómez-Gesteira, R.A. Dalrymple; 2007; 3D SPH Simulation of large waves mitigation with a dike; *Journal of Hydraulic Research*(45,5):631-642.
16. Crespo A.J.C., J.M. Domínguez, B.D. Rogers, M. Gómez-Gesteira, S. Longshaw, R. Canelas, R. Vacondio, A. Barreiro, O. García-Feal; 2015; DualSPHysics: Open-source parallel CFD solver based on Smoothed Particle Hydrodynamics (SPH); *Computer Physics Communications*, 187:204-216.
17. Crespo A.J., M. Gómez-Gesteira, R.A. Dalrymple; 2008; Modeling Dam Break Behavior over a Wet Bed by a SPH Technique; *Journal of Waterway, Port, Coastal, and Ocean Engineering*, 134(6):313-320; DOI: 10.1061/(ASCE)0733-950X(2008)134:6(313)
18. Di Monaco A., S. Manenti, M. Gallati, S. Sibilla, G. Agate, R. Guandalini; 2011; SPH modeling of solid boundaries through a semi-analytic approach. *Engineering Applications of Computational Fluid Mechanics*, 5(1):1-15.
19. Engage Digitizer (Mitchell et al.), <https://github.com/markummitchell/engage-digitizer>

- 1
2
3
4
5
6
7
8
9
10
11
12
13
14
15
16
17
18
19
20
21
22
23
24
25
26
27
28
29
30
31
32
33
34
35
36
37
38
39
40
41
42
43
44
45
46
47
48
49
50
51
52
53
54
55
56
57
58
59
60
61
62
63
64
65
20. Ferrand M., D.R. Laurence, B.D. Rogers, D. Violeau, C. Kassiotis; 2013; Unified semi-analytical wall boundary conditions for inviscid laminar or turbulent flows in the meshless SPH method; *International Journal for Numerical Methods in Fluids*, 71(4):446-472.
 21. Free Software Foundation <http://www.fsf.org/>
 22. GDAL (OSGEO); <https://github.com/OSGeo/gdal>
 23. Gnuplot (Williams & Kelley), <http://www.gnuplot.info/>
 24. Gomez-Gesteira M., B.D. Rogers, R.A. Dalrymple, A.J.C. Crespo; 2010; State-of-the-art of classical SPH for free-surface flows; *Journal of Hydraulic Research*, 48(Extra Issue):6-27; doi:10.3826/jhr.2010.0012
 25. GSView (Ghostgum Software Pty Ltd), <https://www.ghostscript.com/>
 26. Gu S., X. Zheng, L. Ren, H. Xie, Y. Huang, J. Wei, S. Shao; 2017; SWE-SPHysics simulation of dam break flows at South-Gate Gorges Reservoir; *Water (Switzerland)*, 9(6), art. no. 387.
 27. Hashemi M.R., R. Fatehi, M.T. Manzari; 2012; A modified SPH method for simulating motion of rigid bodies in Newtonian fluid flows; *International Journal of Non-Linear Mechanics*, 47:626–638.
 28. Image Magick (ImageMagick Studio LLC), <https://www.imagemagick.org>, last access on 28May2019
 29. Khayyer A., Gotoh H., Falahaty H., Shimizu Y.; 2018; An enhanced ISPH–SPH coupled method for simulation of incompressible fluid–elastic structure interactions; *Computer Physics Communications*, 232:139-164.
 30. Kumaran V.; 2015; Kinetic theory for sheared granular flows; *C. R. Physique* 16:51-61.
 31. Le Touzé D., A. Colagrossi, G. Colicchio, M. Greco; 2013; A critical investigation of smoothed particle hydrodynamics applied to problems with free-surfaces; *Int. J. Numer. Meth. Fluids*, 73:660-691; DOI: 10.1002/fld.3819
 32. Lobovsky L., E. Botia-Vera, F. Castellana, J. Mas-Soler, A. Souto-Inglesia; 2014; Experimental investigation of dynamic pressure loads during dam break; *J. Fluid Struct.*,48:407-434.

- 1
2
3
4
5
6
7
8
9
10
11
12
13
14
15
16
17
18
19
20
21
22
23
24
25
26
27
28
29
30
31
32
33
34
35
36
37
38
39
40
41
42
43
44
45
46
47
48
49
50
51
52
53
54
55
56
57
58
59
60
61
62
63
64
65
33. Macia F., L.M. Gonzalez, J.L. Cercos-Pita; A. Souto-Iglesias; 2012; A Boundary Integral SPH Formulation - Consistency and Applications to ISPH and WCSPH-; Progress of Theoretical Physics, 128-3, 439-462.
 34. Manenti, S., Amicarelli, A., Todeschini, S.; 2018; WCSPH with Limiting Viscosity for Modeling Landslide Hazard at the Slopes of Artificial Reservoir. Water, 10(4), 515; doi:10.3390/w10040515.
 35. Manenti S., S. Sibilla, M. Gallati, G. Agate, R. Guandalini; 2012; SPH Simulation of Sediment Flushing Induced by a Rapid Water Flow; Journal of Hydraulic Engineering ASCE 138(3): 227-311.
 36. Marongiu J.C.; F. Leboeuf, J. Caro, E. Parkinson; 2010; Free surface flows simulations in Pelton turbines using an hybrid SPH-ALE method; J. Hydraul. Res., 47:40–49.
 37. Mayrhofer A., B.D. Rogers, D. Violeau, M. Ferrand; 2013; Investigation of wall bounded flows using SPH and the unified semi-analytical wall boundary conditions; Computer Physics Communications, 184: 2515-2527.
 38. Monaghan JJ. Smoothed particle hydrodynamics; 2005; Rep. Prog. Phys., 68:1703–1759.
 39. OpenFOAM (OpenCFD Ltd), <https://github.com/OpenFOAM/OpenFOAM-dev> (last access on 28May2019), <https://github.com/isoAdvector/isoAdvector> (last access on 28May2019)
 40. Paggi M., M. Ciavarella; 2010; The coefficient of proportionality κ between real contact area and load, with new asperity models; Wear (268,7-8):1020-1029.
 41. Paggi M., Q.-C. He; 2015; Evolution of the free volume between rough surfaces in contact, Wear (336–337):86-95.
 42. Paraview (Kitware), <https://github.com/Kitware/ParaView>
 43. Price, D.J.; 2012; Smoothed Particle Hydrodynamics and Magnetohydrodynamics; J. Comp. Phys., 231(3): 759-794.

- 1
2
3
4
5
6
7
8
9
10
11
12
13
14
15
16
17
18
19
20
21
22
23
24
25
26
27
28
29
30
31
32
33
34
35
36
37
38
39
40
41
42
43
44
45
46
47
48
49
50
51
52
53
54
55
56
57
58
59
60
61
62
63
64
65
44. Rendina I., G. Viccione, L. Cascini; 2019; Kinematics of flow mass movements on inclined surfaces; *Theoretical and Computational Fluid Dynamics*, 1-17, in press, doi: 10.1007/s00162-019-00486-y
 45. Rexer M., C. Hirt; 2014; Comparison of free high resolution digital elevation data sets (ASTER GDEM2, SRTM v2.1/v4.1) and validation against accurate heights from the Australian National Gravity Database, *Australian Journal of Earth Sciences*, 61(2):213-226, DOI: 10.1080/08120099.2014.884983
 46. Sarno L., L. Carleo, M.N. Papa, P. Villani; 2018; Experimental investigation on the effects of the fixed boundaries in channelized dry granular flows. *Rock Mechanics and Rock Engineering*, 51(1):203-225. doi: 10.1007/s00603-017-1311-2
 47. Schaeffer D.G.; 1987; Instability in the Evolution Equations Describing Incompressible Granular Flow; *Journal of Differential Equations*, 66:19-50.
 48. Shadloo M.S., G. Oger, D. Le Touzé; 2016; Smoothed particle hydrodynamics method for fluid flows, towards industrial applications: Motivations, Current state, And challenges; *Computers and Fluids*, 136:11-34.
 49. SPHERA (RSE SpA), <https://github.com/AndreaAmicarelliRSE/SPHERA>, last access on 28May2019
 50. SPHERIC (SPH scientific and industrial community affiliated to ERCOFTAC -European Research Community On Flow, Turbulence and Combustion-), <http://spheric-sph.org/> (last access on 28May2019), <http://spheric-sph.org/sph-projects-and-codes> (last access on 28May2019)
 51. Rendina I., G. Viccione, L. Cascini; 2019; Kinematics of flow mass movements on inclined surfaces; *Theoretical and Computational Fluid Dynamics*, 1-17, in press, doi: 10.1007/s00162-019-00486-y
 52. SRTM3/DTED1 (USGS); <http://earthexplorer.usgs.gov/> (last access on 28May2019)
 53. Terzaghi, K.; 1943; *Theoretical soil mechanics*; New York, London: Wiley.

- 1
2
3
4
5
6
7
8
9
10
11
12
13
14
15
16
17
18
19
20
21
22
23
24
25
26
27
28
29
30
31
32
33
34
35
36
37
38
39
40
41
42
43
44
45
46
47
48
49
50
51
52
53
54
55
56
57
58
59
60
61
62
63
64
65
54. Vacondio R, Rogers BD, Stansby P, Mignosa P.; 2012; SPH Modeling of Shallow Flow with Open Boundaries for Practical Flood Simulation; J. Hydraul. Eng., 138(6):530–541.
55. Van Rijn L.C.; 1993; Principles of sediment transport in rivers, estuaries, and coastal seas; Aqua Publications.
56. Viccione G., B. Tagliaferro; 2018; Simulating dry granular flow with dualsphysics; Proc. of the 5th IAHR Europe Congress - New Challenges in Hydraulic Research and Engineering, Eds. Aronne Armanini and Elena Nucci, Trento, 13-15 June 2018, Italy: 401-402, doi: 10.3850/978-981-11-2731-1_316-cd
57. Vila J.P.; 1999; On particle weighted methods and Smooth Particle Hydrodynamics; Mathematical Models and Methods in Applied Sciences, 9(2):161-209.
58. Violeau D.; A. Leroy; 2014; On the maximum time step in weakly compressible SPH; Journal of Computational Physics, 256: 388-415.
59. Violeau D., B.D. Rogers; 2016; Smoothed particle hydrodynamics (SPH) for free-surface flows: past, present and future; Journal of Hydraulic Research, 54(1):1-26.
60. Virtual Dub (Avery Lee), <http://www.virtualdub.org/> (last access on 28May2019)